AD NUMBER

AD911533

NEW LIMITATION CHANGE

TO

Approved for public release, distribution unlimited

FROM

Distribution authorized to U.S. Gov't. agencies only; Test and Evaluation; MAR 1973. Other requests shall be referred to Air Force Avionics Laboratory, Attn: TEA, Wright-Patterson AFB, OH 45433.

AUTHORITY

AFAL ltr, 20 Jan 1976

TECHNICAL REPORT AFAL-TR-73-58

COMPARATIVE PERFORMANCE OF HOLLOW-CATHODE AND AXIAL PLASMA HELIUM-NEON LASERS

H.G. Heard, Principal Investigator

A.J. Palmer, Project Engineer

Air Force Avionics Laboratory
Aeronautical Systems Division
Wright-Patterson Air Force Base, Ohio

PREPARED BY

INFORMATION SYSTEMS

4020 CAMPBELL AVENUE
MENLO PARK, CALIFORNIA 94025
415-323-8301

NOTICE

When Government drawings, specifications, or other data are used for any purpose other than in connection with a definitely related Government procurement operation, the United States Government thereby incurs no responsibility nor any obligation whatsoever; and the fact that the government may have formulated, furnished, or in any way supplied the said drawings, specifications, or other data, is not to be regarded by implication or otherwise as in any manner licensing the holder or any other person or corporation, or conveying any rights or permission to manufacture, use, or sell any patented invention that may in any way be related thereto.

Copies of this report should not be returned unless return is required by security considerations, contractual obligations, or notice on a specific document.

TECHNICAL REPORT AFAL-TR-73-58

COMPARATIVE PERFORMANCE OF HOLLOW-CATHODE AND AXIAL PLASMA HELIUM-NEON LASERS

H.G. Heard, Principal Investigator
A.J. Palmer, Project Engineer

IS-R-73/03 Copy of

PREPARED BY

INFORMATION SYSTEMS

4000 CAMPBELL AVENUE
MENLO PARK, CALIFORNIA 94025
415 323 8301

A DIVISION OF MBASSOCIATES

FOREWORD

This report was submitted January 10, 1973 and covers a 12 month research program entitled Comparative Performance of Hollow-Cathode and Axial Plasma Helium-Neon Lasers was carried out during the period from December 15, 1971 to December 15, 1972.

MBA/Information Systems
4000 Campbell Ave.
Menlo Park, Calif. 94025

under contract No. F33615-72C-1323

The program was monitored by Dr. W. F. Schuebel, Capt. J. Moonan, and Major Robert Owens of the Advanced Electronics Branch, Air Force Avionics Laboratory, Wright-Patterson Air Force Base, Ohio.

Publication of this report does not constitute Air Force approval of the report's findings or conclusions. It is published only for the exchange and stimulation of ideas.

Reviewed and Approved:

Approved Robert D. Larson

Robert D. Larson
Chief, Advanced Electronic Devices Branch
Electronic Technology Division
Air Force Avionics Laboratory

ABSTRACT

This report covers a 12 month, primarily experimental investigation of the comparative performance characteristics of slotted hollow-cathode and axial plasma (positive column) 6328Å He-Ne lasers. The program included the evaluation of parameters that control power performance and culminated in the construction of a TEM_{oo} mode power-optimized slotted hollow-cathode laser. The program was carried out in three main phases. First, a 15 mW TEM_{oo} mode power-optimized axial plasma laser was constructed utilizing a 1-meter long folded confocal laser cavity. Second, a series of systematic parametric evaluations on the 6328Å laser oscillation of He-Ne-slotted hollow-cathode discharges using various cathode diameters was carried out using the same type of laser cavity. Among the most important observations made in this phase were: the inability, due to plasma expulsion from the cathode interior, to reach optimal operating pressure for maximum 6328Å output, consequently the power output and efficiency were lower than that of the 6328Å axial plasma laser; a sensitive dependence of performance on fractional slot width to cathode area; a quasi-periodic distribution of discharge erosion along the length of the cathode slot; and a comparatively high optimal He:Ne mixture ratio. Third, on the basis of the parametric evaluations, a TEM_{oo} mode power-optimized slotted hollow-cathode laser was constructed using a 1-meter long folded-confocal laser cavity. The performance characteristics of this laser were: maximum TEM_{oo} mode output power of 2 mW, optimal total operating pressure of 4 Torr, a He:Ne mixture ratio of 20:1 and nominal discharge current and tube voltage of 400 mA and 220 volts respectively.

TABLE OF CONTENTS

TABLE OF CONTENTS

LIST OF ILLUSTRATIONS

LIST OF ILLUSTRATIONS

LIST OF TABLES

I INTRODUCTION

Among the several possible regions and configurations of a gas discharge which may serve to maintain population inversion in gases, by far the most commonly utilized has been of the positive column region in both glow and arc discharges, with the column axis aligned collinearily with the optic axis of the laser cavity. This configuration is hereafter referred to as an axial-plasma laser (APL). In recent years, much attention has been directed towards alternative plasma configurations which may offer special advantages. One of the most successful of these is the family of new transient, transverse-excited atmospheric pressure (TEA) lasers. At the low pressure end of the spectrum, encompassing the neutral gas, rare-gas ion, and metal-vapor ion lasers, a transverse-glow discharge configuration is rapidly gaining interest of investigators. This configuration has apparent advantages inherent in both the plasma physics and engineering qualities of the discharge. The configuration studied herein is the hollow-cathode laser (HCL). In this discharge inversion is excited in the negative glow region.

To date most of the HCL applications have been to the metal-vapor, rare-gas lasers. Improved electron energy distribution, and reduction of cataphoretic-pumping inhomogeneities, are specific HCL advantages compared to the APL.

This report covers a 12-month investigation, the broad objectives of which were to evaluate and optimize the performance of a 6328Å He-Ne slotted hollow-cathode laser. A further objective was to compare the HCL operating characteristics with those of an optimized APL. The primary motivation of the program was to determine if the slotted hollow-cathode, 6328Å He-Ne laser could offer an attractive solution to the need for a ruggedized, low voltage, low beam wander laser.

Section II below reviews the theory and design features of a 6328Å He-Ne axial plasma laser. A user-interactive computer program, APL, included in Appendix II, was developed to determine the design parameters for a TEM_{oo} power optimized 6328Å He-Ne axial plasma laser.

Section III introduces the concept of the slotted hollow-cathode discharge and contrasts the basic engineering and plasma physics differences between it and the axial plasma discharge.

Section IV briefly reviews the design and operating characteristics of a slotted hollow-cathode He-Ne laser constructed identical to the original HCL built by W. F. Schuebel, hereafter referred to as the "Schuebel Equivalent" Tube.[1]

Section V summarizes the principal measurements on a variety of parameters as carried out with the hollow-cathode laser test facility. The objective of this phase of the work was to identify scaling laws that characterize the 6328Å He-Ne slotted hollow-cathode laser.

In Section VI a theoretical model is synthesized that gives analytic form to scaling relations that are consistent with the measurements for small-bore tubes. A user-interactive computer model, HCL, included in Appendix IV, paralleling that for the axial plasma laser, was developed for designing a TEM_{oo} power-optimized slotted hollow-cathode laser.

Construction details of an optimized slotted hollow-cathode laser are given in Section VII and performance comparisons between this laser and the optimized axial plasma laser are presented in Section VIII.

Section IX draws conclusions and makes recommendations based upon this work concerning possible methods for improving power and efficiency from 6328Å hollow-cathode lasers.

Finally, Appendices are included which present the computer program listings and a calibration curve relative to optical gain measurements.

II THE OPTIMIZED AXIAL PLASMA LASER

The 6328Å He-Ne APL, because it is the oldest gas laser, is one of the most thoroughly studied commercially available APL's. The well documented theory of the axial plasma is reviewed briefly below. Pertinent results are incorporated in a user-interactive computer program, APL$_o$, that can be utilized to tabulate the design parameters for a specified 6328Å laser output. A general description of the optimized APL which was constructed for the performance comparison studies of Section 8 is also included.

2.1 Plasma Characteristics

He-Ne axial plasma lasers utilize the positive column plasma of a glow discharge. This is a wall-stabilized plasma, whose axial extent stretches between the anode and Faraday dark space regions of the discharge, is illustrated in Figure 1. The electron-energy distribution is Maxwellian in the positive column. The electron temperature maintains itself at a value, which balances the production of ions, by electron collisions, with the loss of ions, by ambipolar diffusion, to the walls. This is the well known Schottky model[1] of the positive column. The Schottky model leads to the important scaling laws, which state that, to first order, the electron temperature and axial electric field are, for a given gas, functions of the product of tube diameter times pressure. Specifically[1],

$$\exp(eV_i/kT_e) \;/\; (eV_i/kT_e)^{1/2} = C_1(pD)^2 \qquad (2.1\text{-}1)$$

$$E/p = C_2T_e \qquad (2.1\text{-}2)$$

where V_i is the ionization potential of the gas, k is Boltzmann's constant, C_1 and C_2 are characteristic constants of the gas, p is the pressure, D is the tube diameter, T_e is the electron temperature and E is the axial electric field.

For a given He-Ne mixture and at a fixed discharge current the maximum laser gain at 6328Å occurs at close to a constant value of (pD), and, therefore, at close to a constant value of the electron temperature. With an optimal mixture ratio of He:Ne ≈ 7:1, the empirical relationship is[2]

$$(pD)_{opt.} = 3.6 \text{ Torr - mm} \qquad (2.1\text{-}3)$$

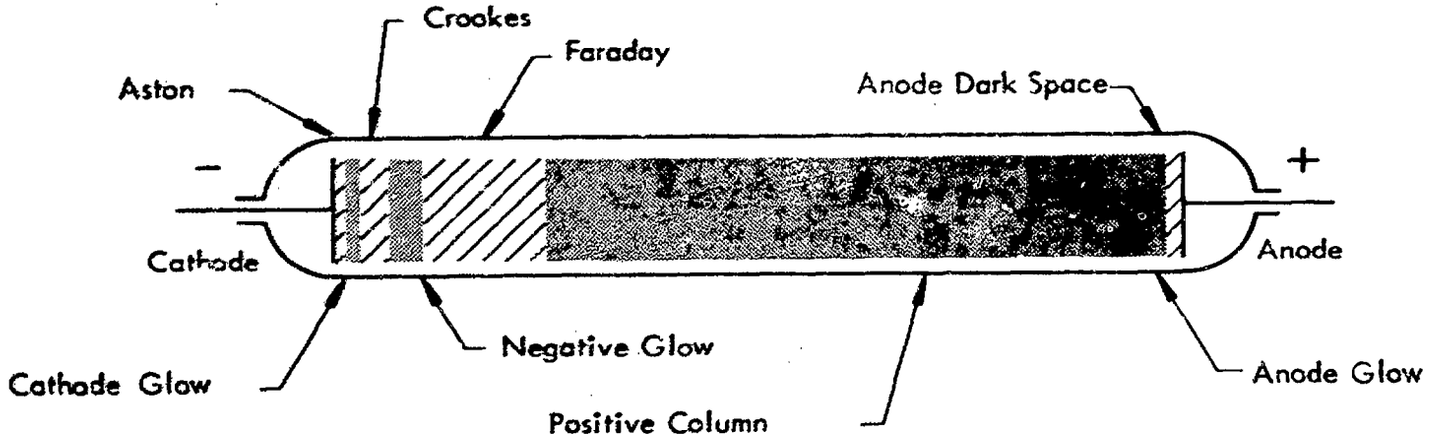

FIGURE 1
REGIONS OF A GLOW DISCHARGE

The discharge current optimizes at a value[2]

$$I_{opt.}\,(mA) = 3.5 + 1.5D^2 \qquad (2.1\text{-}4)$$

with D in mm, and corresponds, except for very small bores, to a constant current density and, therefore, constant electron density. Above this limit de-excitation processes begin to saturate the inversion. In view of Eq. (2.1-3), one expects the gain, under optimal conditions, to increase inversely with the tube diameter since smaller tubes permit proportionally larger operating pressures and consequent larger inversion densities. The empirical relationship for the gain coefficient is[3]

$$g = 3.0/D \text{ percent/meter} \qquad (2.1\text{-}5)$$

with D in cm. An approximate 50 percent increase in the gain and output power can be accomplished by suppressing oscillation of the high gain 3.39μm line which competes strongly with 6328Å emission by depleting the upper laser level. This can be conveniently accomplished by splitting the lower level for the 3.39μm transition with about a 100 gauss inhomogeneous magnetic field.[4]

2.2 Cavity Optimization

Consider the multi-axial mode, single transverse TEM_{oo} mode operation. There are two main considerations to be addressed in optimizing the optical cavity design of a 6328Å He-Ne laser. One is, of course, the optimization of output coupling. The other is diffraction losses as they relate to the dependence of the TEM_{oo} mode dimensions and optical-cavity parameters.

The Boyd & Gordon relations, which express the minimum spot size, w_o and the spot size at the mirrors, $w_{1,2}$ in terms of the mirror radii of curvature, R_1 and R_2 and the mirror separation, d are significant. The symmetric resonator, using mirrors of equal radii of curvature, leads to[5]:

$$w_0 = \left(\frac{\lambda}{\pi}\right)^{1/2} \left(\frac{d}{2}\right)^{1/4} \left(R - \frac{d}{2}\right)^{1/4} \qquad (2.2\text{-}1)$$

$$w_{1,2} = \left(\frac{\lambda d}{2\pi}\right)^{1/2} \left(\frac{2R^2}{d(R-d/2)}\right)^{1/4} \qquad (2.2\text{-}2)$$

where λ is the radiation wavelength. The value of R (for a given d) for which the mirror spot size is a minimum is readily found from Eq. (2.2-2) to be R = d. For this important condition the cavity reduces to the symmetric confocal geometry and Eqs. (2.2-1) and (2.2-2) become

$$(\omega_0)_{conf.} = \left(\frac{\lambda d}{2\pi}\right)^{1/2} \tag{2.2-3}$$

and

$$(\omega_{1,2})_{conf.} = (\omega_0)_{conf.} \sqrt{2} \tag{2.2-4}$$

The beam geometry for this case is illustrated in Figure 2.

Relationships (2.2-3) and (2.2-4) can also be used to describe the mode geometry of a folded confocal cavity. That is a cavity in which a flat mirror is placed at the center of symmetry as shown in Figure 2. In this case, d in Eq. (2.2-3) is replaced by 2 d' where d' is the mirror separation of the folded confocal cavity. The minimum spot size, ω_0 then occurs at the flat mirror. It may appear that, for a given mirror separation, the confocal geometry is not the most efficient as it leads to a cone shaped mode. In a cylindrically shaped plasma tube, a cone does not fill the volume. It turns out, however, that the geometry has been found to be more efficient. The folded confocal geometry was used throughout this investigation.

It has been determined experimentally that a diffracting aperture of approximately 4 times the beam spot size will introduce appreciable diffraction loss for higher order modes while allowing the TEM_{00} mode to propagate. In view of the fact that the gain increases reciprocally with the diameter, it is advantageous, for single transverse mode operation to design the plasma tube of the smallest possible diameter consistent with maintaining low diffraction loss, hence, with a tube diameter of $\sim 4W_{1,2}$.

Appendix I contains the listing of a user-interactive CAV computer program that uses Eq. (2.2-4) to calculate the spot size versus mirror separation for a confocal and folded confocal cavity for 6328Å. The program computes the optimal tube diameter to use for maximum TEM_{00} mode output power. An example output for D = 100 cm is shown which specifies a tube diameter of 0.254 cm for the folded confocal cavity laser constructed for the comparison studies of Section VIII.

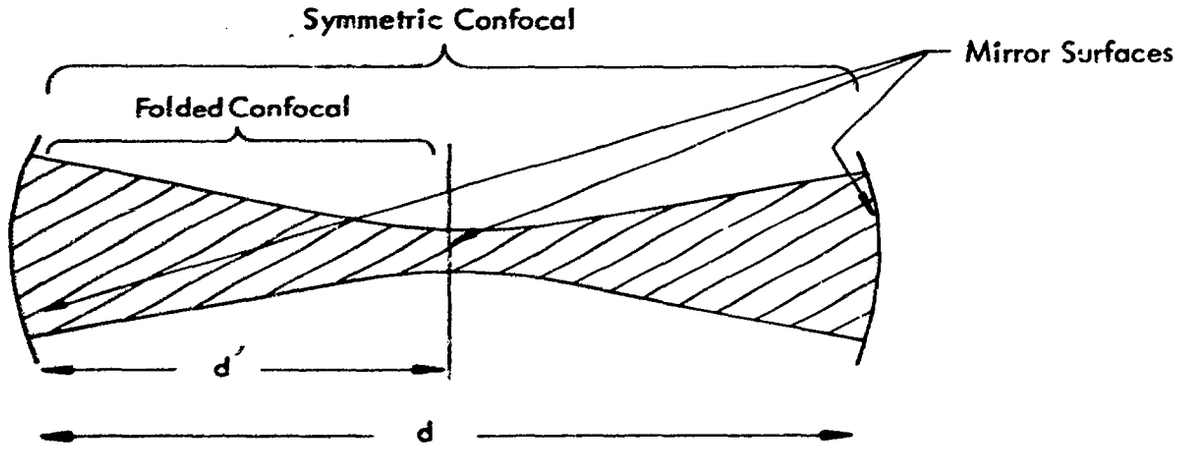

FIGURE 2
MODE GEOMETRY OF SYMMETRIC CONFOCAL AND
FOLDED CONFOCAL OPTICAL RESONATORS

The problem of optimum output coupling in a 6328Å He-Ne laser was considered in detail sometime ago.[5] For a laser with small fractional loss per pass, the oscillations will stabilize at a level where the saturated gain at the oscillation frequency is just equal to the losses. At this point, the output power density from a four level laser such as the 6328Å He-Ne laser transition is,

$$P = T P_{sat} \left(\frac{G}{A + T} - 1\right) \qquad (2.2\text{-}5)$$

where T is the output-mirror transmission, P_{sat} is the saturation power density of the transition, ($P_{sat} = 30 \pm 3$ watts/cm^2 for He-Ne 6328Å), G is the gain per pass through the plasma, and A is the total loss per pass through the cavity, excepting the output coupling. The optimal value for T is found by differentiation and is given by

$$Topt/2G = A/G \ (1 - A/G) \qquad (2.2\text{-}6)$$

for which case the maximum output power density is

$$P_{max} = P_{sat} G(1 - A/G)^2 . \qquad (2.2\text{-}7)$$

These formulas have been incorporated in APL to facilitate the design of a 6328Å He-Ne axial plasma laser. The program listing is presented in Appendix II. It takes as input, the values for plasma length, loss coefficient, output mirror transparency, and the plasma tube diameter from which it calculates the maximum gain coefficient from Eq. (2.1-5). The output tabulates optimum mirror transparency, the output power density, and the power density for other mirror transparencies. The 1-meter long 2.3 mm plasma tube specified for optimal TEM_{oo} operation is required by the computer program CAV, to have an optimum mirror transparency is shown to be approximately 3.9 percent.

2.3 The Optimal Axial Plasma Laser

A photograph of the axial plasma laser which was constructed in accordance with the above optimal design specifications shown in Figure 3. A schematic illustration of the plasma and resonator configuration is shown in Figure 4.

As illustrated, two axial discharges are run from a common aluminum "cold" cathode. Each anode has a separate ballast resistor of 150 kΩ each. The tube is fitted with two 1/8" thick, 1/10 wave flat opposing quartz brewster windows. The geometry centered the tube inside a folded confocal resonator with 1-meter mirror separation. The flat mirror transmissivity was ≤ 0.04 percent. The 2-meter radius spherical output mirror had a 3.5 percent transmission.

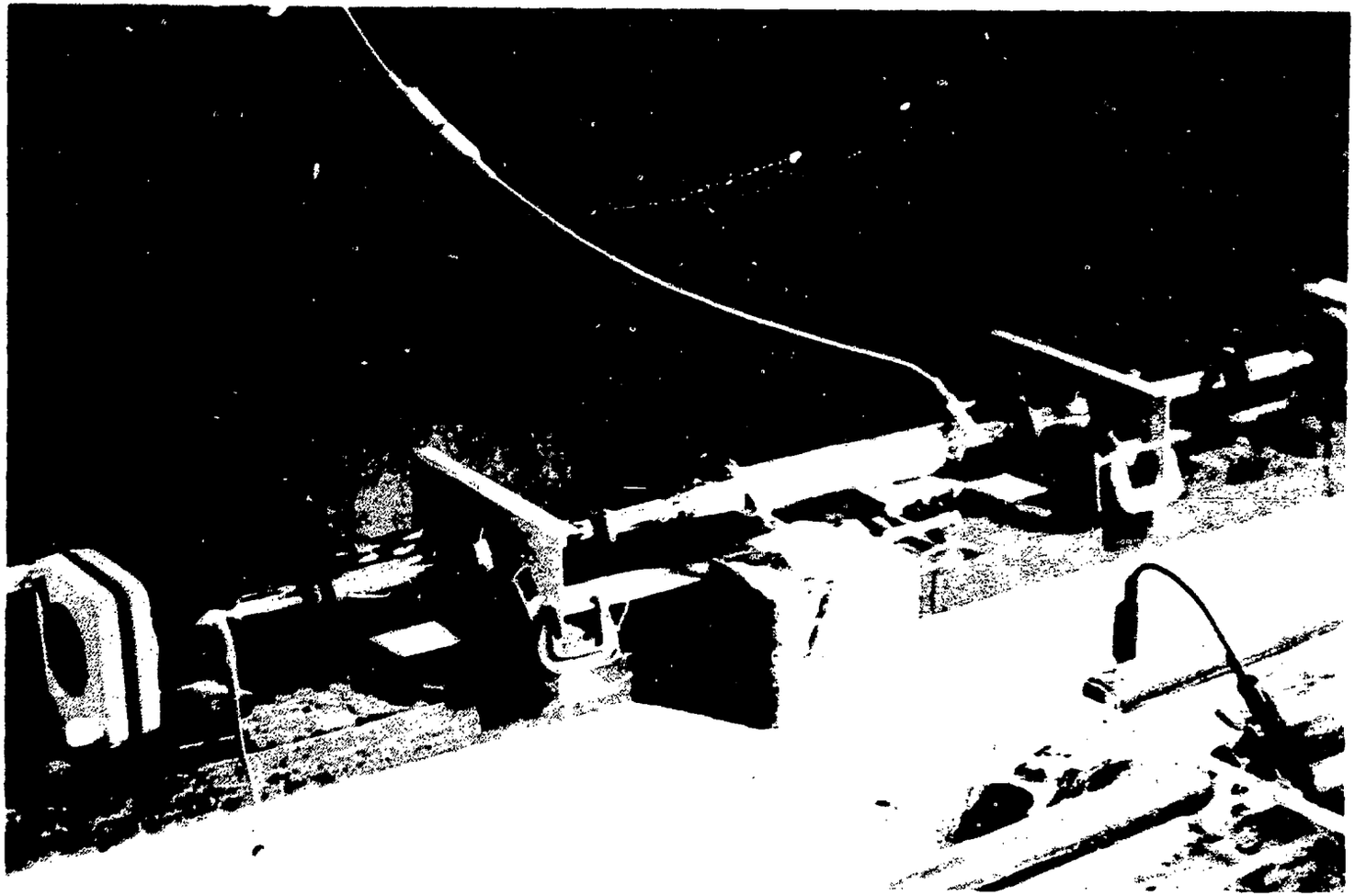

FIGURE 3
PHOTOGRAPH OF AXIAL PLASMA LASER

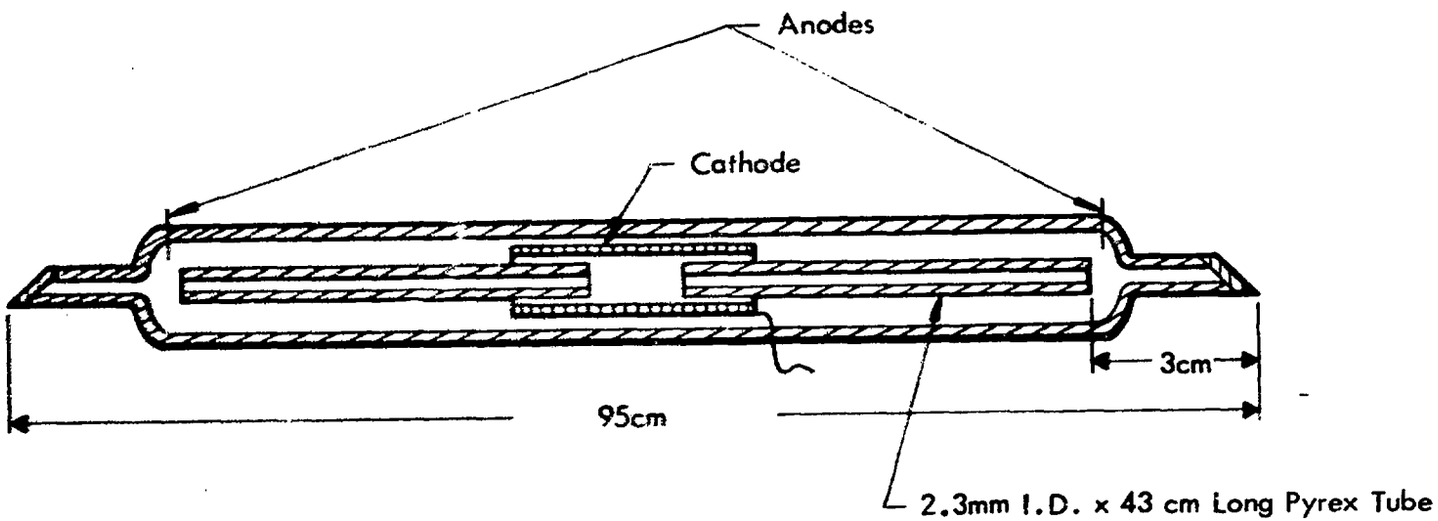

FIGURE 4
SCHEMATIC ILLUSTRATION OF AXIAL PLASMA LASER

III THE SLOTTED HOLLOW-CATHODE DISCHARGE

Figure 5 shows the plasma configuration of a slotted hollow-cathode glow discharge for two different operating pressures. The plasma, which forms inside the cathode, is the negative-glow plasma shown in Figure 1. The plasma establishes itself near the cathode, and will form at a thickness and distance from the cathode that is a function of the pressure, cathode potential fall, and type of gas. The cathode potential fall occurs across the Crookes dark space region between the cathode surface and the cathode-side boundary of the negative glow. The negative-glow plasma itself is an essentially field-free region with the current through the plasma being carried primarily by diffusion. The positive column is absent in these discharges. The region between the negative glow and the anode is occupied at high pressures only by the Faraday dark space and a short anode region. In any case the potential drop across these regions is quite small compared to that across the Crookes dark space. The cathode drop is nominally 200 - 300 volts in the HCL. This constitutes essentially the entire tube voltage. In the APL the cathode drop is usually a small fraction of the total tube drop, nominally 1 - 2 kv. Most of the tube voltage develops along the axis of the positive column.

The thickness of both the negative glow plasma and of the Crookes dark space decrease with increasing pressure. Figure 5b depicts the visible glow of the plasma at a pressure high enough to contract the Crookes dark space and negative-glow region to transverse dimensions that are small relative to the cathode internal diameter. In this situation, the electrical characteristics of the cathode discharge are essentially those of a plane cathode. This geometry is not suitable for a laser plasma. When the pressure is low enough for the negative glow from opposite sides of the cathode to overlap, as in Figure 5a both the electrical and optical properties of the discharge are markedly improved. Much larger currents can be driven through the discharge as the result of enhanced secondary emission efficiency. Increased concentrations of ions and metastables build-up in the negative glow. This is an important characteristic for improved laser excitation.

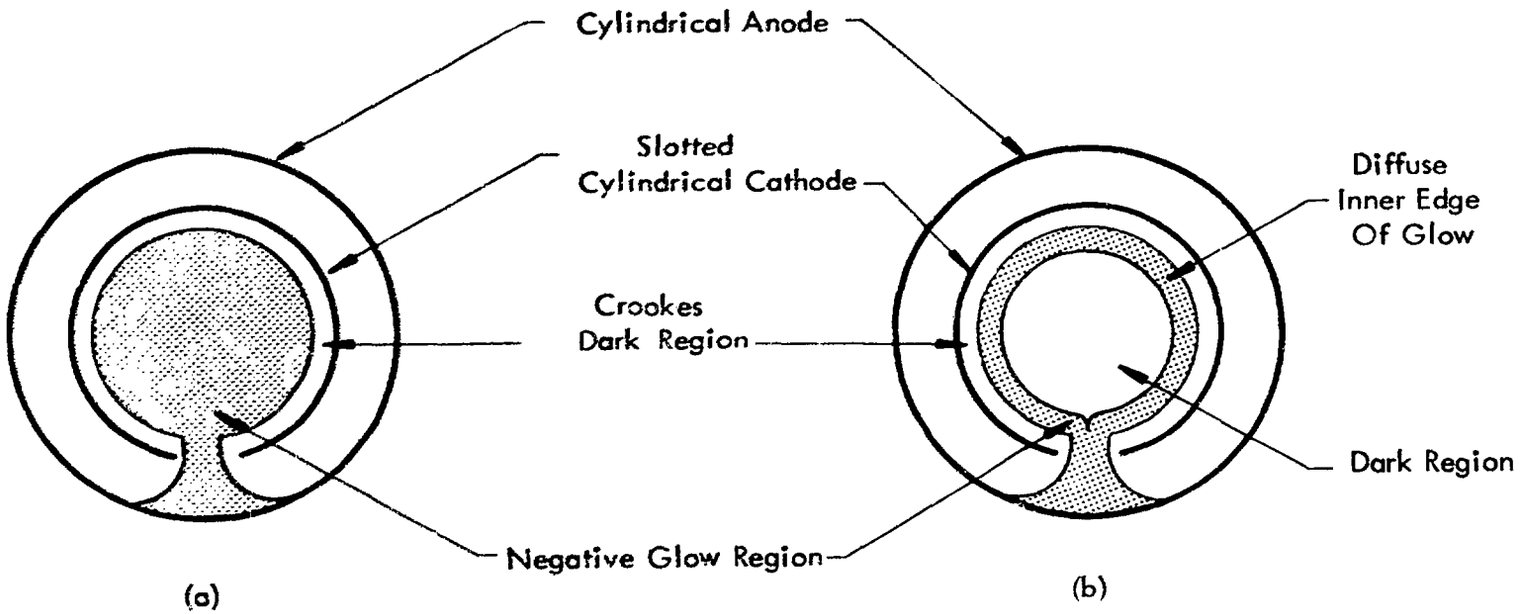

FIGURE 5
CROSS-SECTION VIEW OF ELECTRICAL DISCHARGE IN A SLOTTED HOLLOW CATHODE UNDER CONDITIONS OF a) LOW GAS PRESSURE, AND b) HIGH GAS PRESSURE

It is clear that there will be a minimum operating pressure below which the transverse dimensions of the cathode region become too large to be compatible with stable operation in the cathode interior. It is observed experimentally that efficient performance of the 6328Å He-Ne laser transition requires, unfortunately, operating pressures at values where this instability occurs.

The anode-cathode spacing is chosen small enough to preclude the discharge from running off the outside surface of the cathode, yet not so small that shorting or arcing occurs. The slot width is chosen to allow maximum internal cathode surface area without causing severe Crookes -layer discharge blockage. A more quantitative discription of this latter constraint will be taken up in Section VI.

IV THE "SCHUEBEL EQUIVALENT" HOLLOW-CATHODE LASER

In order to establish a standard for comparing the work done on this program with the earlier work done by W. F. Schuebel on 6328Å He-Ne slotted hollow-cathode lasers, a slotted hollow-cathode laser tube was constructed that modeled the original geometry employed in Schuebel's early studies.[1] The tube also proved useful in life testing of a sealed-off tube and for examining cathode-material-dependent effects.

A photograph and schematic illustration of the tube is shown in Figures 6 and 7 respectively. The brewster windows were identical to those used on the axial plasma laser. A 1-meter-long folded confocal resonator with a .04 percent transmission flat reflector and a 0.4 percent transmission, 2-meter radius output mirror was used.

Prior to taking measurements the tube was baked at 100°C at pressures below 10^{-6} Torr until gas evolution ceased to effect operating parameters. Electrical power was supplied to the tube through various ballast resistors typically 100-750 ohms from a 0-800V, 5A variable-output d.c. power supply.

Without the use of a cavity aperture, oscillation at 6328Å occurred simultaneously on several transverse modes. TEM_{oo} mode operation was achieved through the use of a diffracting aperture placed adjacent to the spherical reflector. A power level roughly 1/3 the multimode value was observed. The results of the "Schuebel tube" TEM_{oo} output power measurements are summarized in Figure 8.

As Section V will indicate, a discharge instability occurs as one attempts to increase output power by reducing the pressure. This instability places a limit on the performance of a slotted hollow-cathode He-Ne laser at 6328Å. These preliminary observations are evidently consistent with those made by Schuebel on the 6328Å transition.

Power output instability was also observed, the magnitude of which depended upon how close to the pressure instability one operates. With the tube attached to the vacuum station and having the significant

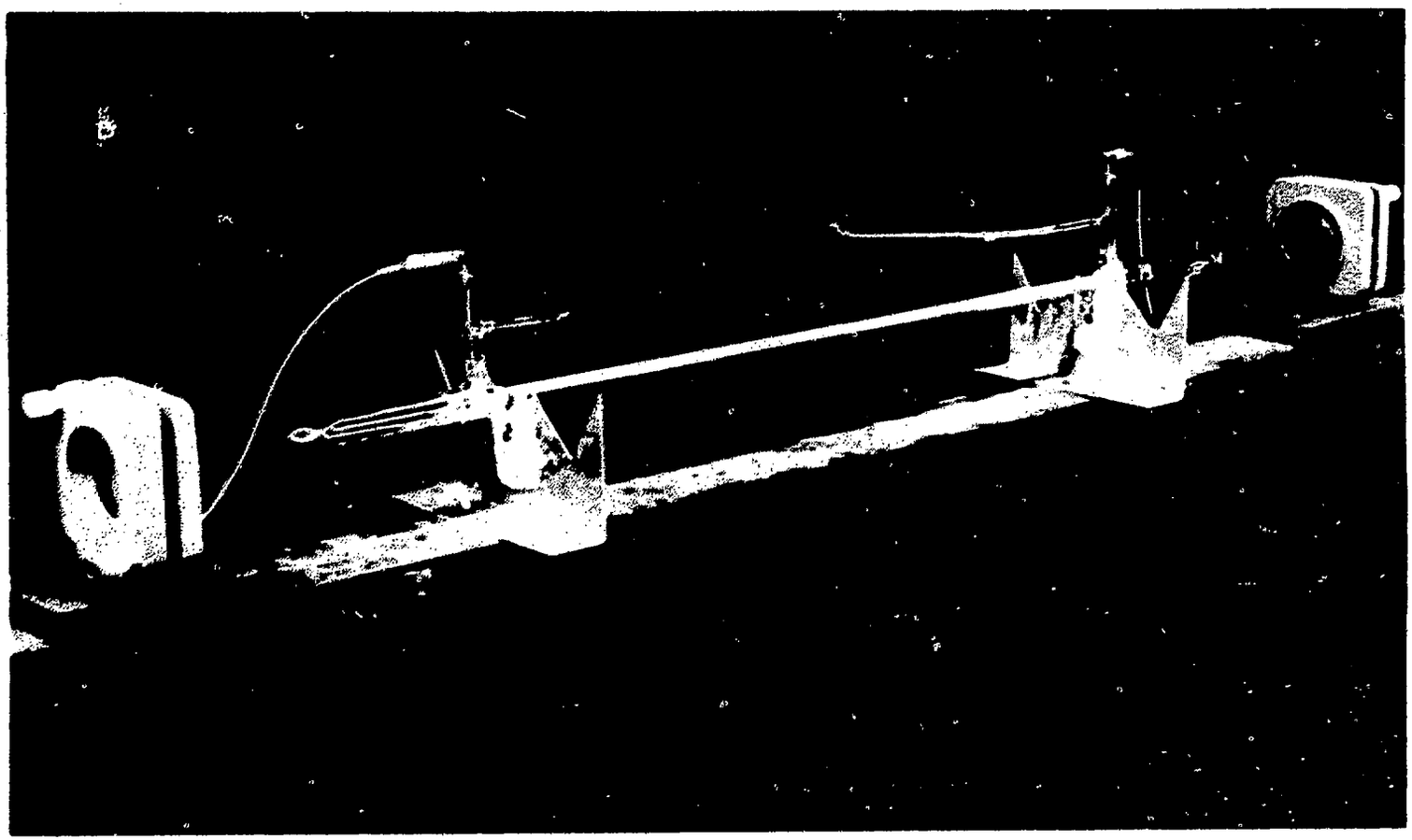

FIGURE 6
PHOTOGRAPH OF "SCHEUBEL EQUIVALENT" SLOTTED HOLLOW-CATHODE LASER

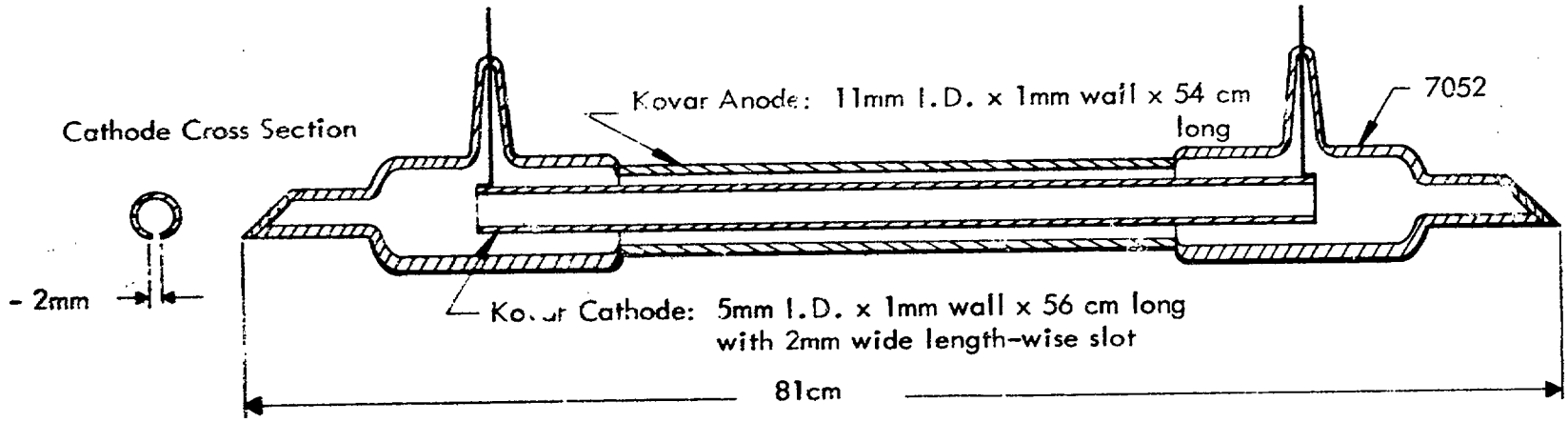

FIGURE 7
SCHEMATIC ILLUSTRATION OF "SCHUEBEL EQUIVALENT"
HOLLOW-CATHODE LASER

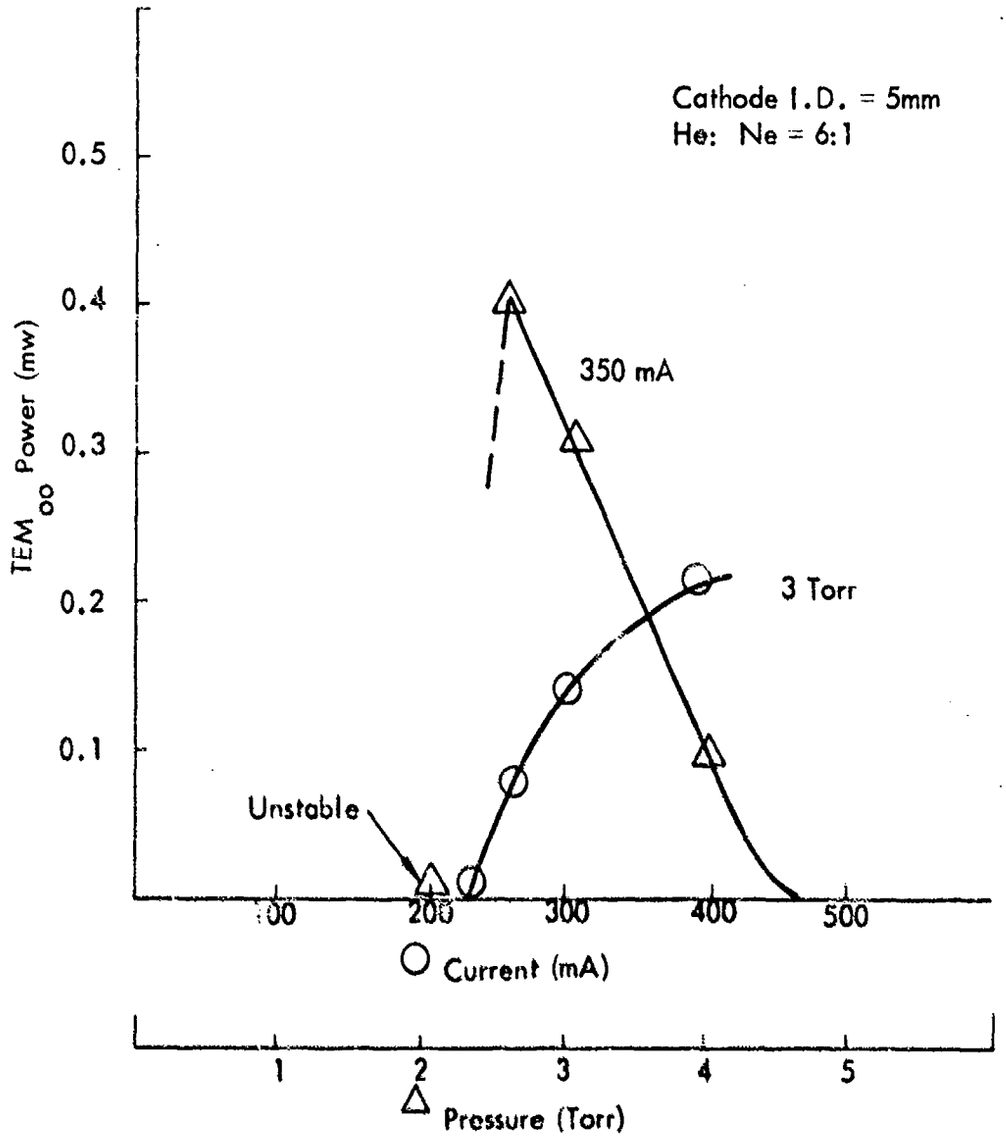

FIGURE 8
DISCHARGE CURRENT & TOTAL PRESSURE
EVALUATIONS - "SCHUELEL EQUIVALENT" TUBE

gas ballast of the pumping station, operation at a pressure of 3 Torr produced reasonably steady output over periods of up to 45 minutes. A tube sealed off at a 3 Torr pressure developed discharge instability and quenching of laser action in less than 15 minutes. Indeed a significant amount of material was sputtered onto the glass sections adjacent to the cathode slot.

V PARAMETRIC EVALUATIONS WITH THE SLOTTED HOLLOW-CATHODE TEST FACILITY

Systematic parametric evaluations of 6328Å He-Ne slotted hollow-cathode laser performance were carried out with a demountable stainless-steel plasma tube capable of accommodating electrodes of various diameters up to ~1.5 inches. A photograph of this test facility is shown in Figure 9. A schematic illustration is shown in Figure 10. The tube's brewster windows were identical to those used on the APL and "Schuebel Equivalent" laser.

This system, as well as the other plasma tubes used in this program, was pumped by an 80 liter/sec. vacuum-ion pump in a station capable of operating at 500° C and 5×10^{-7} Torr. The vacuum station was equipped with a 10 kw, 4 x 8 foot elevating electric oven for discharge-tube baking, and employed a six-port manifold for fill gas mixing. Research grade helium and neon gases were used throughout.

Both aluminum and stainless steel electrode materials were evaluated. The aluminum cathodes, though carefully cleaned, were found to produce extremely unstable discharges. Discharge localization to small regions and excessive heating caused the cathodes to loose rigidity and consequently lead to anode-cathode shorts. It was felt that while a sufficiently elaborate cleaning and baking techniques might be investigated to produce stable discharge behavior with aluminum, the time for the required diversion would be incompatible with a reasonable multiple-diameter electrode evaluation schedule. Thus stainless steel electrodes were used throughout the remainder of this phase of the program.

Electrical power was supplied to the tube from the same power supply used with the "Schuebel Equivalent" tube and was delivered through ballast resistance ranging from 150 - 750 ohms as needed.

For the 5 mm and 8 mm I.D. cathodes the two-point cathode suspension arrangement illustrated in Figure 10 was adequate to maintain the cathode in accurate alignment throughout the range of discharge currents. The 3.5mm and smaller I.D. cathodes, were found to warp

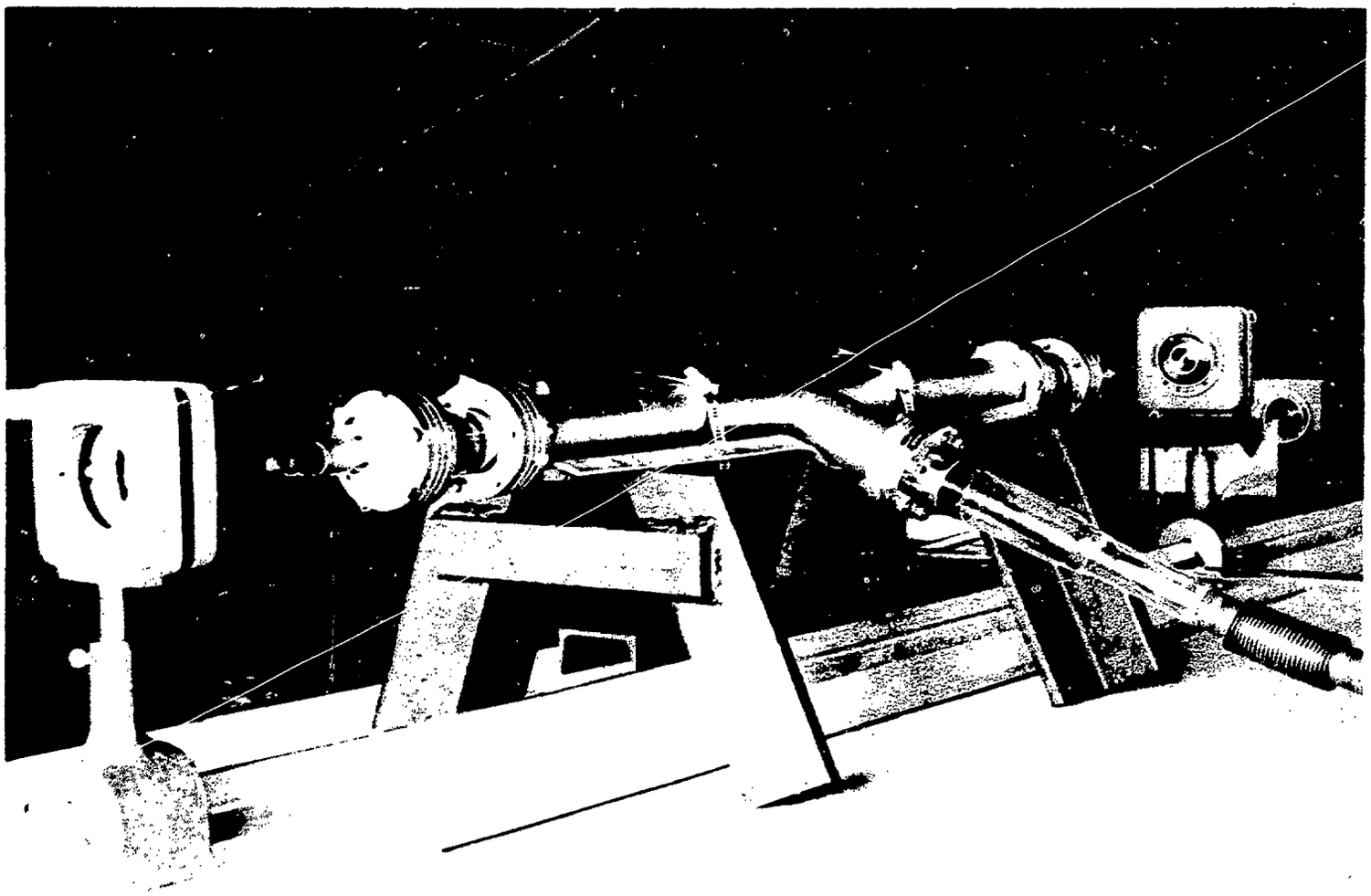

FIGURE 9
PHOTOGRAPH OF HOLLOW-CATHODE LASER "TEST FACILITY" PLASMA TUBE

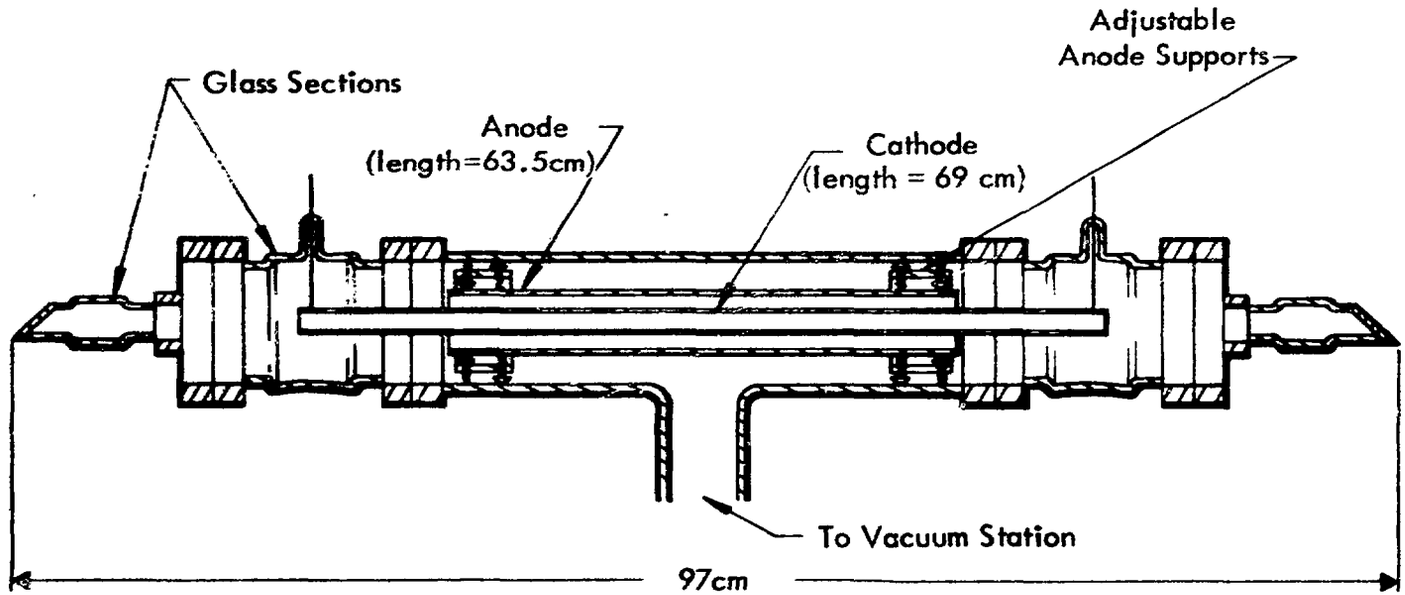

FIGURE 10
SCHEMATIC ILLUSTRATION OF THE "TEST FACILITY" PLASMA TUBE

badly. To overcome this practical problem three co-axial slotted boron nitride sleeves were placed in the cathode-anode space to provide the required additional support.

5.1 TEM_{00} Power vs. Excitation Current and Total Pressure

This section presents the results of the measurements which have the most direct bearing on the scaling behavior of a 6328Å slotted hollow-cathode laser.

Systematic evaluations of the dependence of TEM_{00} output power on excitation current and total pressure were carried out for four different cathode internal diameters between 1.6 and 11 mm. These cathodes had a constant ratio of slot width to cathode I.D. A special cathode was made at 3.5 mm I.D. with two different slot widths. Table I lists the relevant dimensions of the electrode combinations used. Attempts made to achieve laser oscillation with an 11 mm I.D. cathode and with a 1.6 mm I.D. cathode were not successful. The inability to obtain oscillation was due, in the first case, to inadequate gain, and in the second case to severe diffraction losses and plasma instability. The 2.5 to 8 mm range of dimensions was, however, adequate to define the optimal HCL configuration and the important empirical scaling relations.

The data presented in this section are for a constant He-Ne mixture ratio of 6:1. The research grade gas was obtained from a pre-mixed source. The dependencies on gas mixture ratio are presented in Section 5.2 and shown there to be relatively insensitive to cathode diameter.

A 1-meter optical-cavity mirror spacing was used. The mirror geometry was folded confocal and the output mirror transmission was 0.4 percent. An iris was placed near the spherical output reflector to restrict the oscillation to TEM_{00} mode except for the 2.5 mm I.D. cathode. In the latter, the bore diffraction losses were adequate to force single transverse mode operation.

To obtain reproducible values of output power, and preclude a localized discharge, it was always necessary to strike the discharge at high pressure (~20 Torr.) and subsequently reduce the pressure to the range of interest. The discharge could not be restarted reliably at pressures near

TABLE I
ELECTRODE COMBINATIONS

Electrode Set #	Cathode I.D. (mm)	Cathode Slot Width (mm)	Cathode Inside Surface Area (Cm^2)	Anode I.D. (mm)
1	8	3.2	150	14
2	5	1.7	89	11
3a	3.5	1.3	58	7.8
3b	3.5	3.1	46	7.8

Material: Stainless Steel Cathode (Plasma) Length: 63.6 cm
Anode Length: 63.5 cm

the optimum power output.

Uncertainty in the measured data were caused by a downward drift in power during measurements, and low pressure instability. Uncertainty in the optimal pressure is as great as 20 percent. Power output uncertainties were in the range 10 - 15 percent.

The dependence of TEM_{00} output power on total pressure and discharge current for the 3.5mm, 5mm, and 3.8mm I.D. cathodes are shown in Figures 11 through 13. The slot width of each cathode is 40 percent of the cathode I.D. (see Table I). A factor of six reduction in the maximum power output is illustrated by Figure 14 as compared with Figure 13. In Figure 14 the cathode slot width is increased to 90 percent of the 3.5mm cathode I.D. There is a corresponding change in electrical characteristics of this cathode (see Section 5-3).

The power-vs- pressure curves exhibit a low pressure instability limit. This characteristic is always observed when the power is rapidly increasing as the pressure is being reduced. The onset of this instability occurs as the plasma is visually observed to be expelled from the cathode interior. As expected, this transition is accompanied by an abrupt decrease in current and increase in tube voltage. Coincidentally, most of the luminous plasma forms over the exposed end-sections of the cathode. Once this transition begins, the laser output become erratic as indicated by the dashed portion of the power-vs.-pressure plots.

No other abrupt changes were noted in the shape of the individual power-vs.-pressure and power-vs.-current curves, for variations in the respective chosen parametric value of current and pressure, throughout the remaining ranges of interest.

Figures 11 and 13 together show the scaling behavior of the optimum power, defined by the instability, and the corresponding discharge current. The optimum pressure and current decrease and increase respectively with increasing cathode diameter. An analytic model that corresponds with this behavior will be taken up in Section 6.1. Model data consider a constant slot width-to-I.D. ratio.

Another important influence of slot width was observed. All

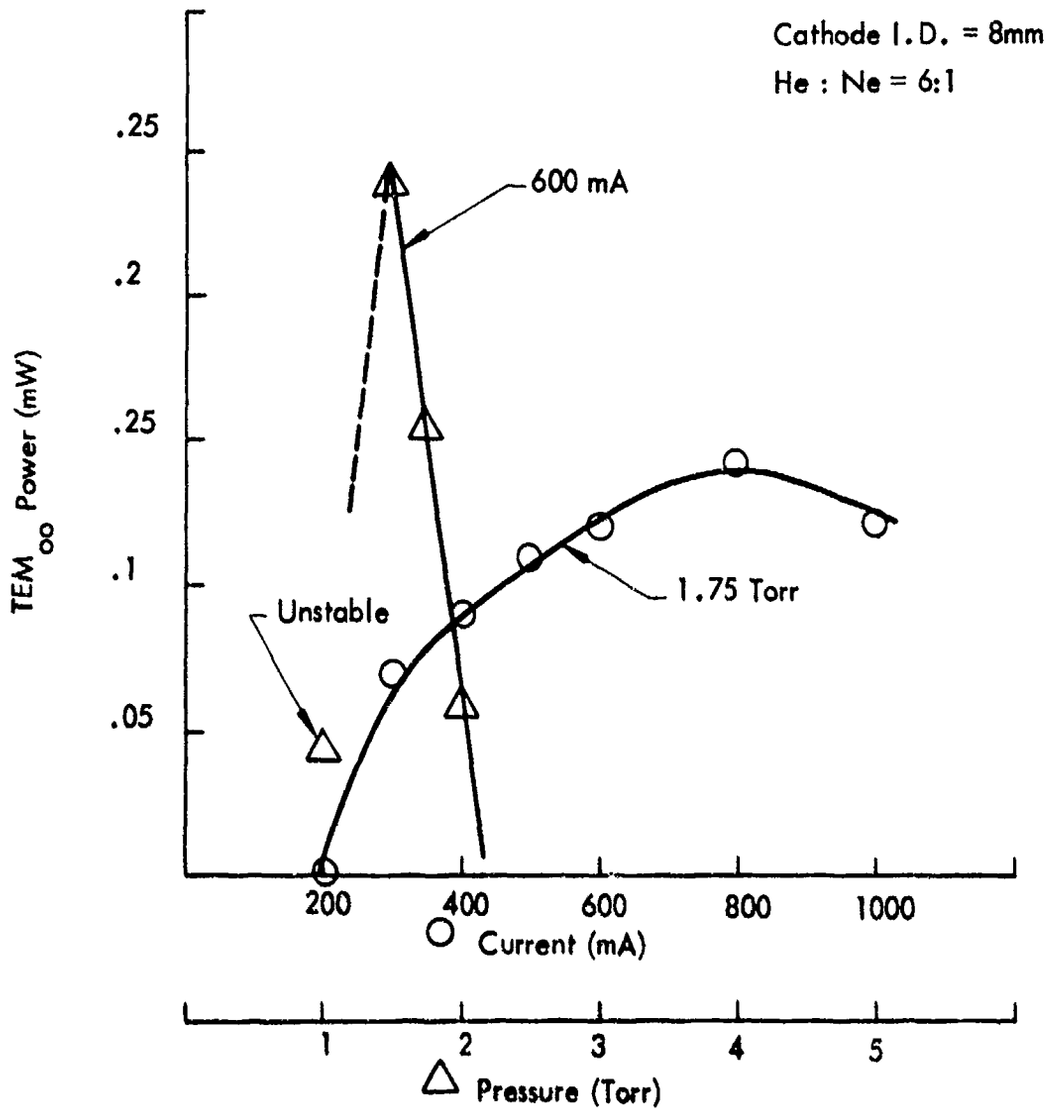

FIGURE 11
DISCHARGE CURRENT & TOTAL PRESSURE
EVALUATIONS - #1 ELECTRODES

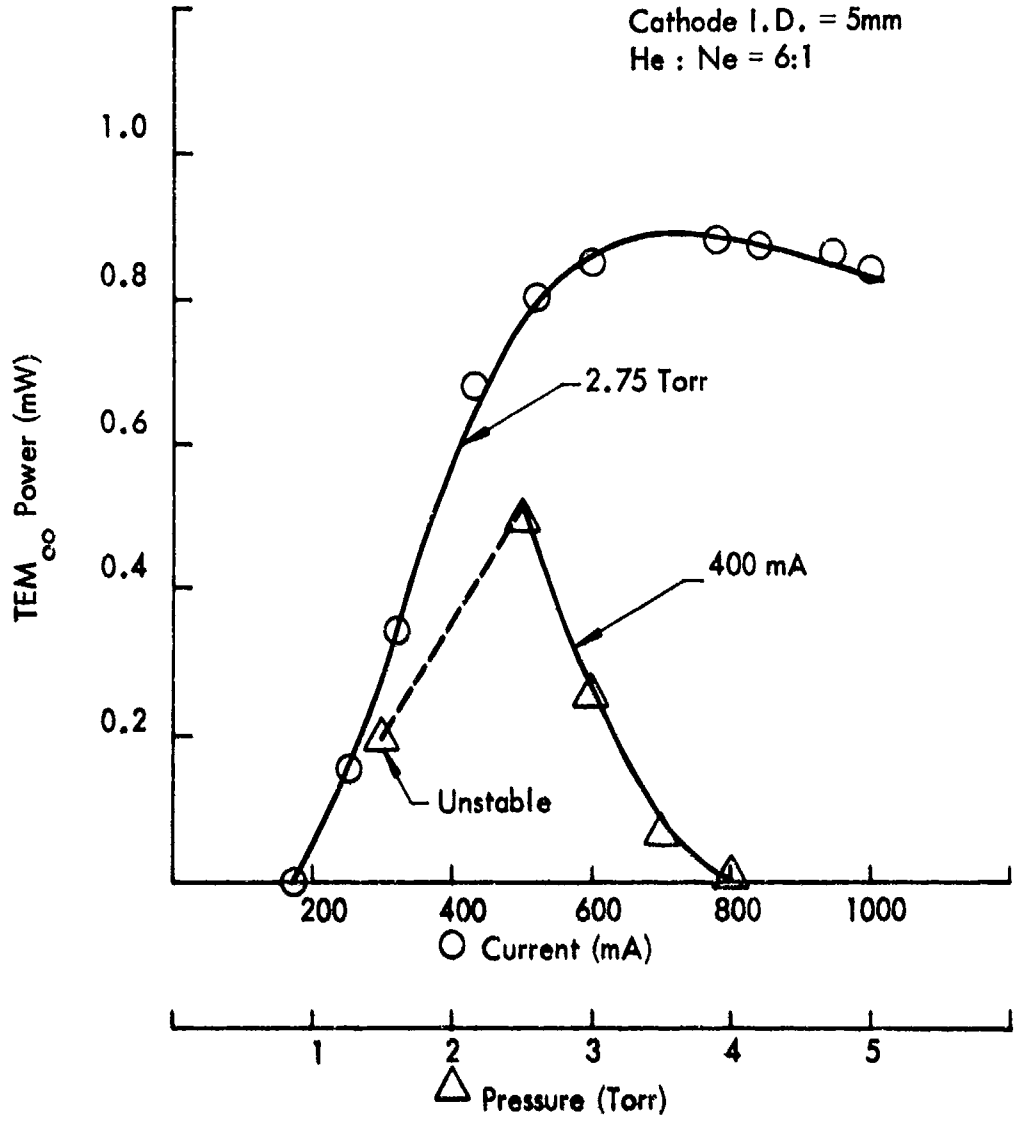

FIGURE 12
DISCHARGE CURRENT & TOTAL
PRESSURE EVALUATIONS - #2 ELECTRODES

MBA
2772-11034

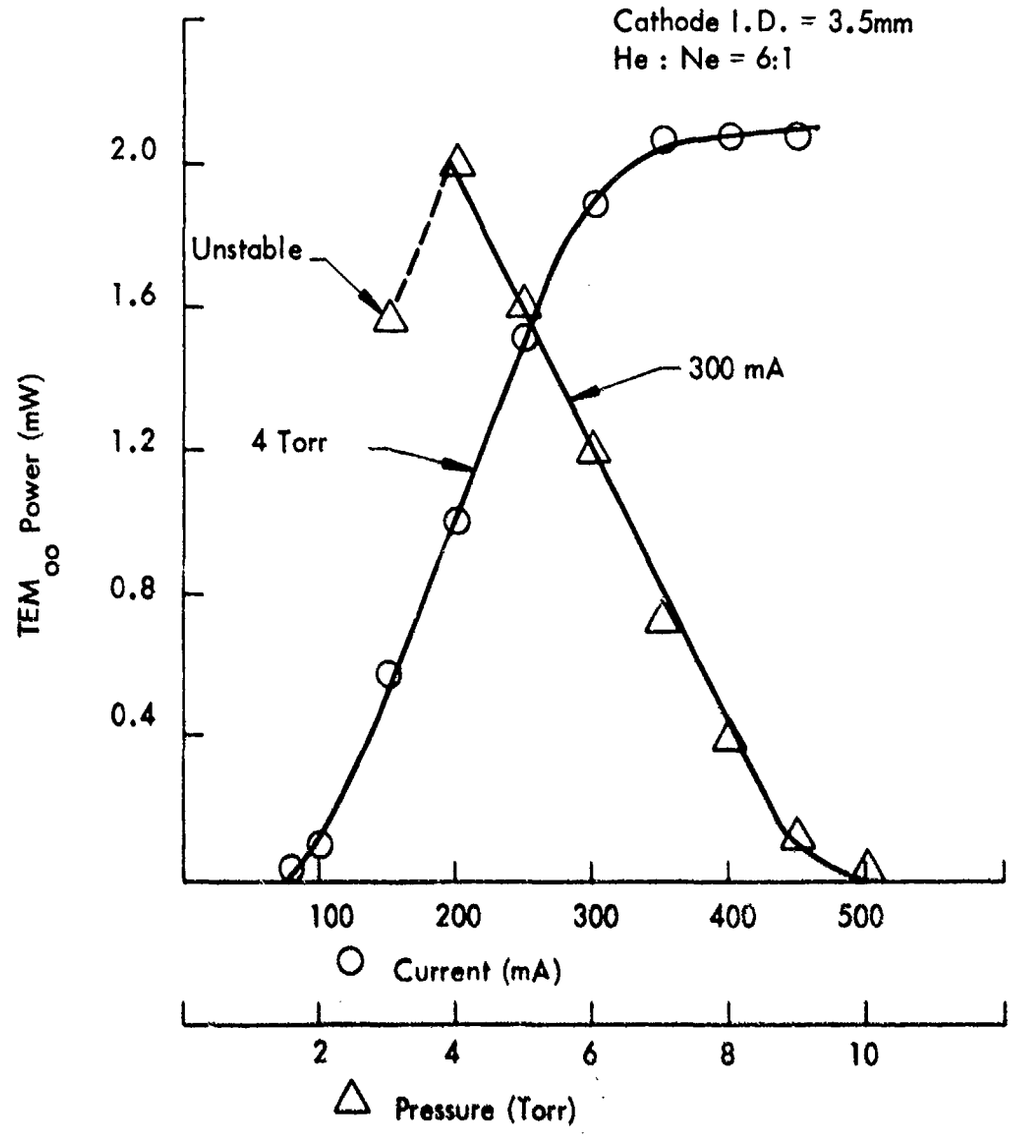

FIGURE 13
DISCHARGE CURRENT & TOTAL
PRESSURE EVALUATIONS - #3a ELECTRODES

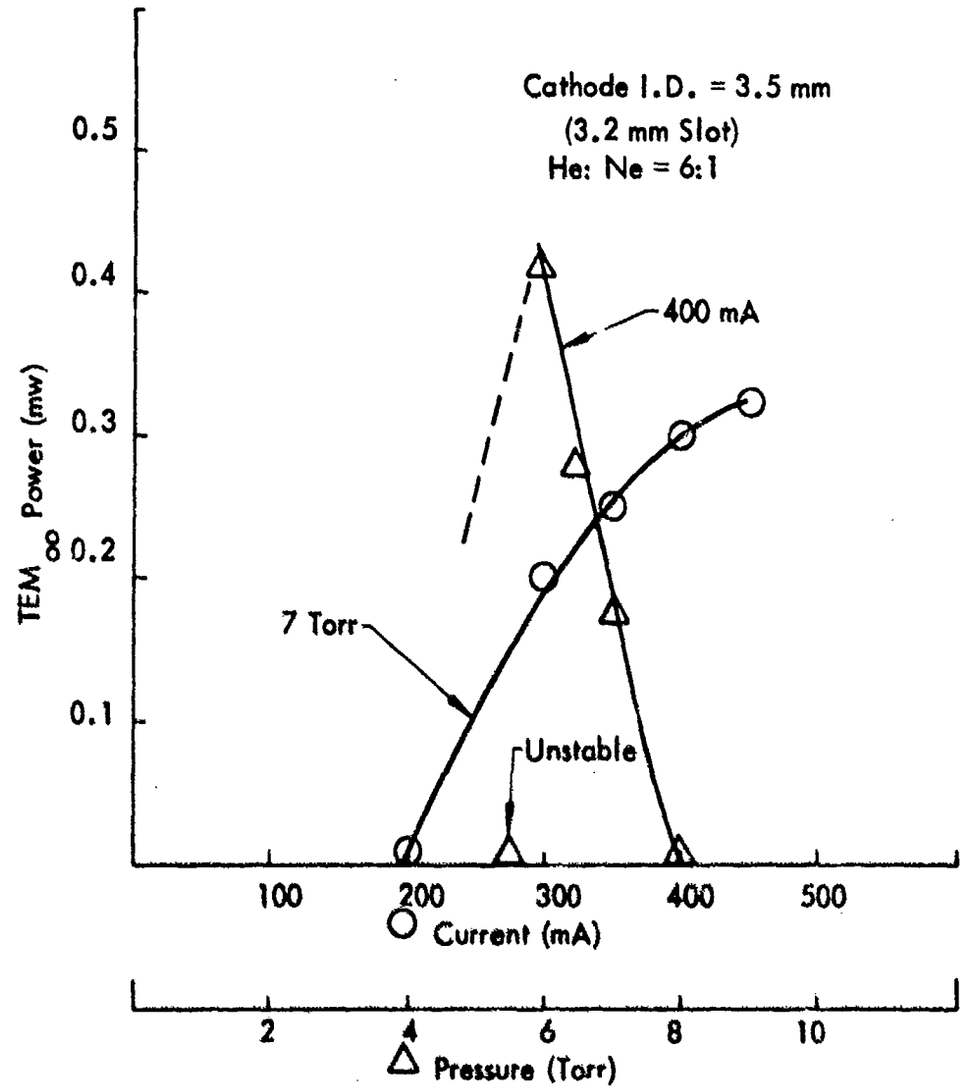

FIGURE 14
DISCHARGE CURRENT & TOTAL PRESSURE EVALUATIONS - #3b ELECTRODES

three cathodes with 40 percent slot width to I. D. ratio exhibited both non-uniform plasma luminosity and cathode erosion. Erosion occurred in a quasi-periodic distribution along the length of the cathode slot. An example of the observed erosion is shown in a photograph for the 5mm I. D. cathode in Figure 15. Average values for the length and spacing of the erosion spots for the three cathodes are indicated in Table II.

The wider slotted cathode used for the data in Figure 14 showed no visible evidence of inhomogeneous discharge formations in the slot. Interpretation of this behavior is offered in Section 6.1.

Laser oscillation at 6328Å was achieved in a 2.5mm I. D. cathode with a 1.2 mm wide slot, using a 5.5 mm I. D. anode. The active cathode length was 45 cm. The slotted cathode was positioned at the small-beam-diameter end of the cavity (near the flat mirrer). TEM_{oo} oscillation occurred without the use of an aperture in this cathode.

No reproducible data could be obtained on either the laser outp or electrical characteristics using this cathode. Both the discharge and the output power were extremely unstable throughout the entire range of pressure where laser action occurred (~6 - 10 Torr). The average value of the output power appeared to increase from 0 to ~0.5 m watts as the pressure was reduced from ~10 to 6 Torr. With the discharge current held approximately constant at ~300 mA the average tube voltage ranged from ~195 to 10 Torr to 250 volts at 6 Torr.

The nature of the discharge instability, which was present throughout this range, was quite different from that of the low pressure plasma explusion. Rather slow (a few seconds) longitudinal motions of localized regions of the plasma were observed to occur within the cathode. The 2.5mm I. D. cathode probably represents a practical lower limit on the slotted hollow-cathode internal diameter. Suggested interpretation of the behavior will be discussed in Section 6.1.

5.2 Partial Pressure Variations

The effect of He:Ne partial pressure variation were investigated for three electrode combinations: #1, #2, and #3a. Data are presented in Figures 16 through 18.

FIGURE 15
CATHODE SPOT EROSION FOR 5 mm I.D. CATHODE

TABLE II
SLOT EROSION PATTERNS

Electrode Set #	Average Erosion Spot Length (mm)	Average Erosion Spot Spacing (mm)	Approximate Number of Spots
1	7	40	10
2	4	30	20
3a	3	20	30

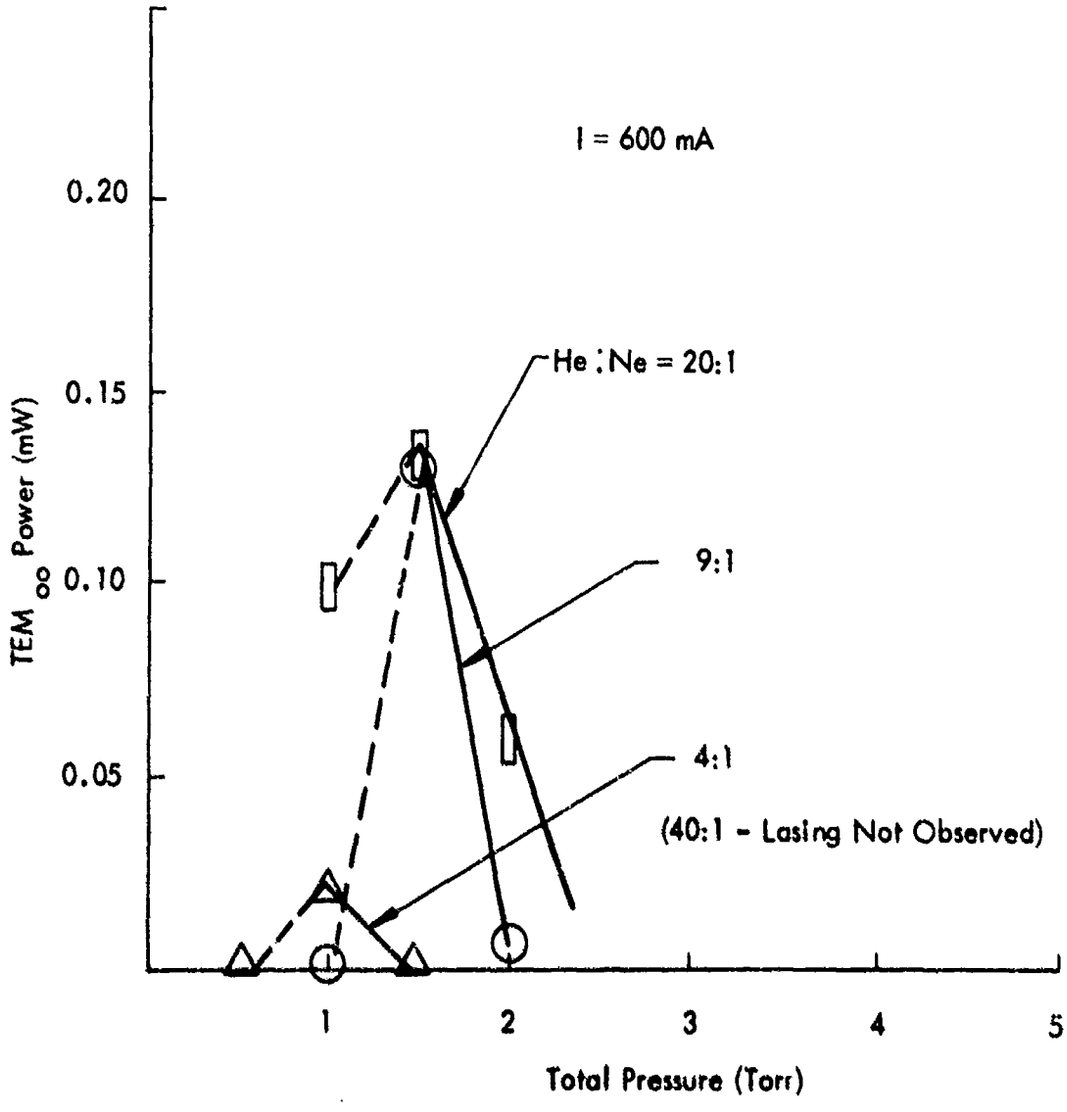

FIGURE 16
PARTIAL PRESSURE EVALUATIONS
- #1 ELECTRODES

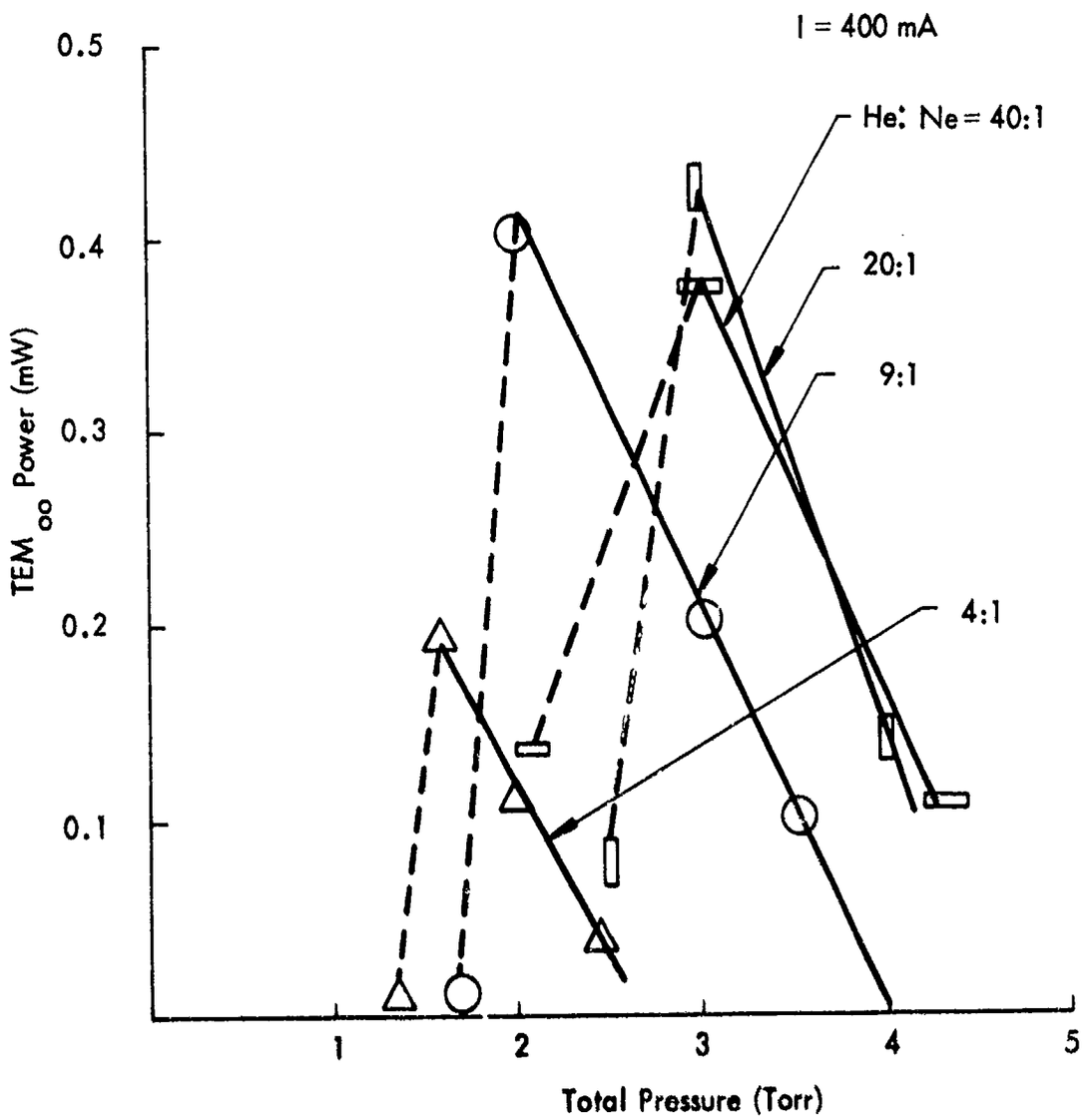

FIGURE 17
PARTIAL PRESSURE EVALUATIONS - #2 ELECTRODES

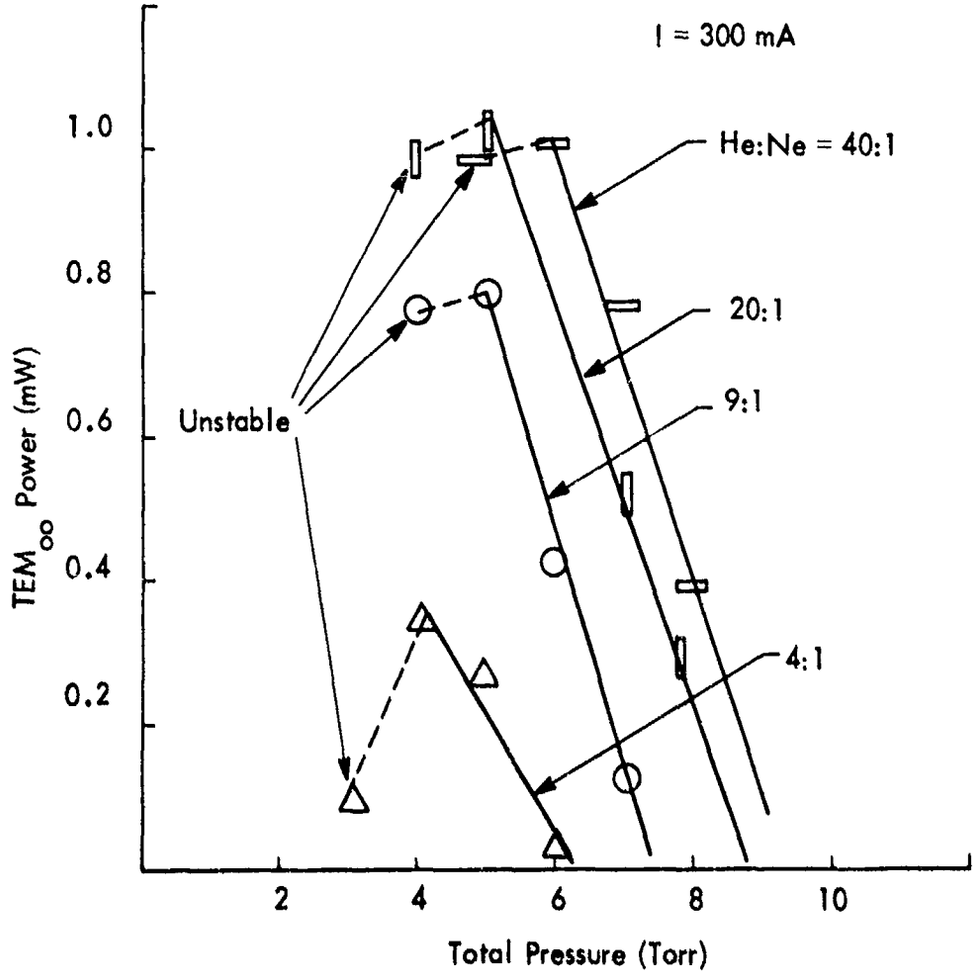

FIGURE 18
PARTIAL PRESSURE EVALUATIONS
-#3a ELECTRODES

The sequential procedures followed in taking these measurements were as follows: a) Fill the tube with helium at 10 Torr; b) add neon to the desired mixture ratio; c) wait at least 5 minutes for mixing (additional mixing time did not introduce observable changes); d) exhaust the tube slowly and measure output power at several pressures between the laser-power output threshold and the pressure at which instability occurs. Discharge current was held constant during measurements. No significant dependence of the mixture ratios on discharge current was noted.

Although optimal He:Ne mixture near 20:1 is apparent, for all three cathodes, a value of 9:1 gives very similar results. The optimal ratio is lower than the corresponding value of 6:1 for the axial plasma 6328Å He-Ne laser. Again the tube performance is relatively insensitive to pressure ratio.

5.3 Current-Voltage Characteristics

Measurements of current-voltage characteristics of the slotted hollow-cathodes are summarized for several geometries in Figure 19 Note that, to first order, all tubes with the same slot width-to-diameter ratio have the same excitation slope. The tube voltage is plotted against reduced current density in accordance with well known similarity laws applicable to the cathode region[1]. Similitude predicts a close-to-linear dependence between the cathode fall voltage over the small range of reduced current densities encountered in these measurements. The reduced current density must, of course, be evaluated at the inside surface of the cathode, and is obtained by dividing the discharge current, by the product of the inside cathode surface area, and the square of the gas pressure.

5.4 Laser Gain and Optimum Mirror Transparency

The problem of obtaining accurate data for laser gain with low-gain laser transitions (such as the 6328Å He-Ne transition) has always been a difficult one. The method of gain measurement chosen, utilized a single 0.5 mm thick variable angle, intercavity, 1/10 wave optical flat. The small thickness was selected to minimize transverse beam displacement. To measure gain the flat was first positioned in the cavity near the

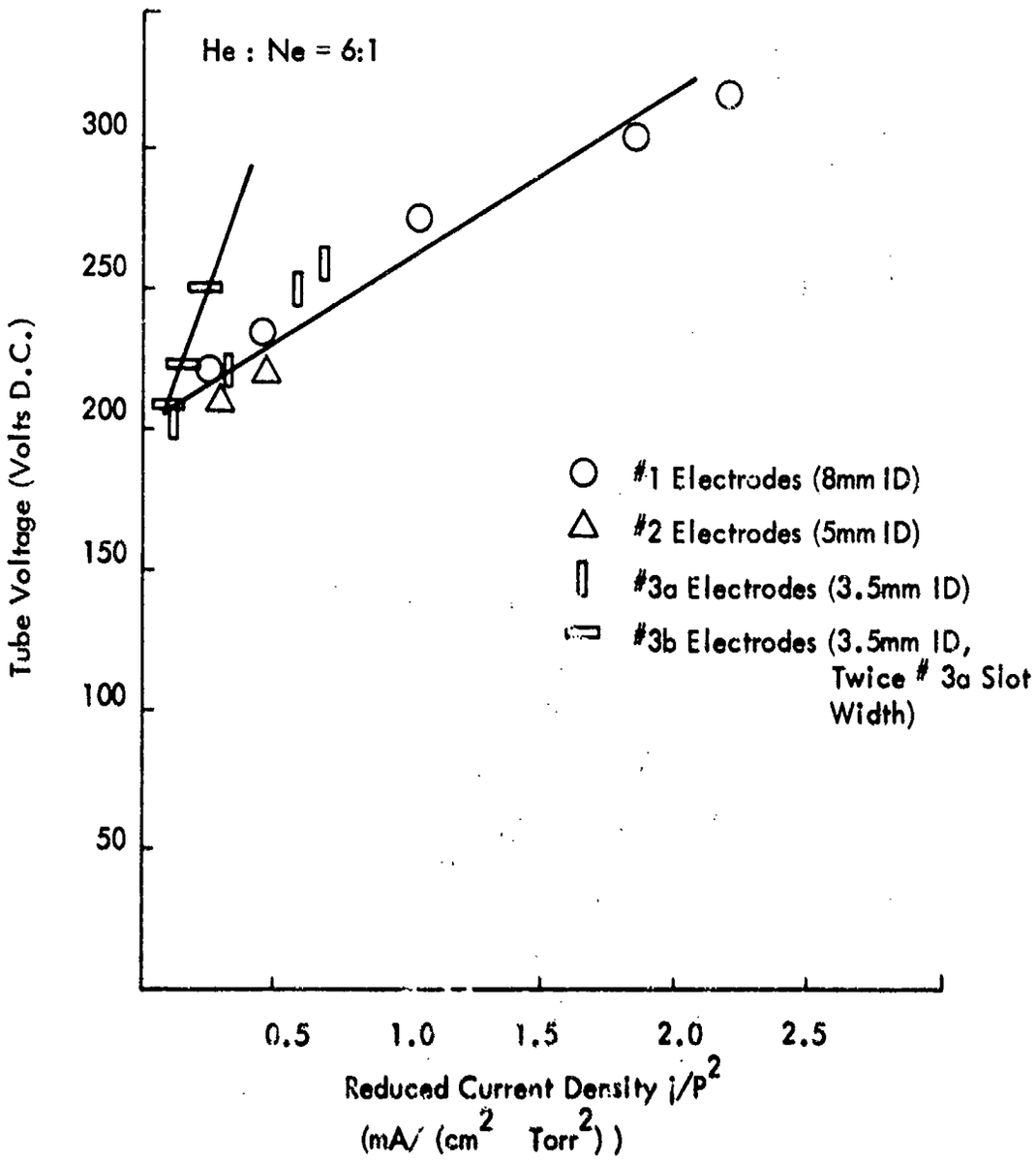

FIGURE 19
CURRENT-VOLTAGE CHARACTERISTICS

output reflector and oriented parallel to the brewster angle window. Beam normality was easily obtained by maximizing laser output with angular position of the flat. The latter was then rotated about an axis normal to the plane of incidence until laser action was extinguished. The angular displacement required to extinguish the beam is related to the round trip excess gain in the cavity. That is the gain is equal to the total losses. Losses consists of surface scattering, mirror transmission, diffraction, and the reflective losses off of the flat.

The usual relation for the Fresnel reflection coefficient[7] cannot be used to calculate the reflection loss as a function of angle due to strong interference effects occurring in the thin flat. The flat was calibrated outside the cavity by measuring reflectance as a function of angle. The calibration curve so obtained is presented in Appendix III.

Gain measurements were taken for the #1, #2, and #3a electrode assemblies each at maximum output power operation. In calculating the gain, an estimate was made of the contribution of scattering to the net loss. An average value of 0.05 percent per window and 0.2 percent per mirror surface was used. For the 8mm I.D. cathode the net scattering loss was comparable to the measured gain. There was a large uncertainty in the gain measurement for this cathode diameter. Three values for gain measurements and corresponding optimal operating pressures are shown in Figure 20 for the 3.5, 5, and 8mm I. D. cathode.

According to Equation 2.2-6, optimal mirror transparency for the 8, 5, 3.5 mm I.D. cathodes are 0.37, 0.55, and 0.79 percent respectively. These values are not inconsistent with an observed reduced output when the mirror was changed from 0.4 percent to 2 percent transparency, the next available transparency increment.

5.5 Magnetic Field Effects

Both homogeneous and inhomogeneous magnetic fields were applied to the test-facility tube. A 12 turn/cm solenoid was wound around the tube jacket and split into four adjacent sections. Current was passed through the sections in opposite directions to provide the inhomogeneous field.

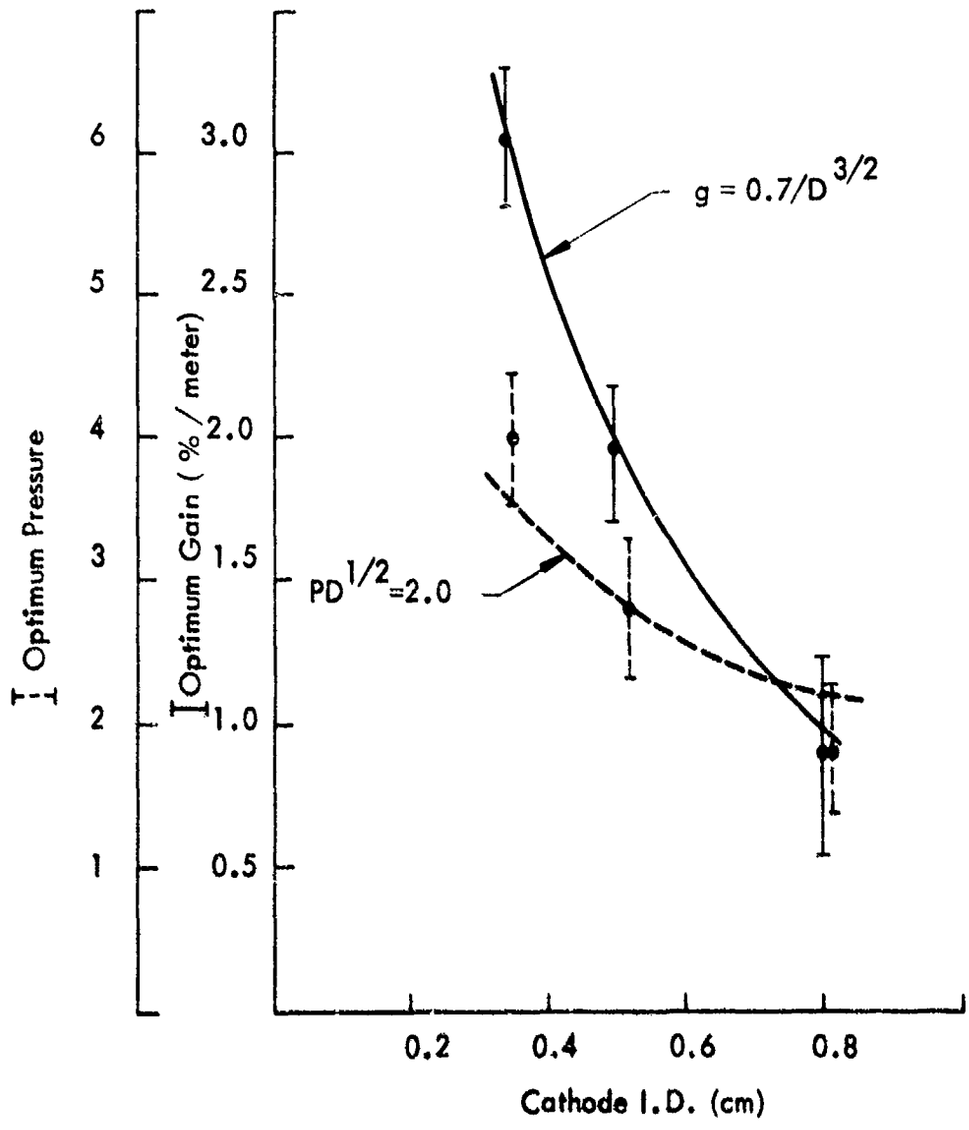

FIGURE 20
OPTIMUM GAIN & PRESSURE- THEORETICAL MODEL COMPARED WITH EXPERIMENT

MBA

2772-11036

It was once conjectured that the application of axial magnetic field to a HCL might not only serve to suppress oscillation at 3.9μm but would also stabilize the plasma at lower pressures. The rational for this projection was that solenoidal field would act upon the high energy electrons, and, contracting in a known fashion[8], the transverse dimension of the cathode regions of the discharge would reduce. Contrary to this concept the observed predominant effect (both homogeneous and inhomogeneous) was to degrade the azimuthal symmetry of the plasma. This doubtless led to a reduced degree of negative-glow overlap. The efficiency of hollow-cathode discharges depend sensitively upon this parameter. A reproducible increase in output power was observed at a field strength near 50 gauss, as shown in Figure 21. The influence of the magnetic field upon the discharge exhibited a hysteresis which may have been caused by gross motion of the cathode spots. In the magnetic field range from 0 to 150 gauss the discharge impedence increased by 5 percent. The influence of either homogeneous or inhomogeneous fields was indistinguishable.

5.6 Doppler Linewidth

Spectral profile measurements were taken with a Tropel Model 242 Scanning Fabry-Perot Interferometer. The instrument has an adjustable free spectral range of from 50 cm^{-1} to 0.03 cm^{-1} (corresponding resolving power of from $>10^3$ to $>5x10^7$) and an aperture limited finesse of >50.

Spectral profiles were obtained for both stimulated and spontaneous emission from the 6328Å transition. The results are presented in Figure 22 for the #3a electrodes. The stimulated emission spectrum shows, as expected, the unstable presence of several simultaneously oscillating axial modes. A meaningful measure of the doppler line-width cannot be obtained from the stimulated line-width data. The hot-cavity line width can only be approximated when oscillation is restricted to a single axial mode. The interferrometer mirror spacing, d, for this case was 1.19 cm corresponding to a free spectral range of:

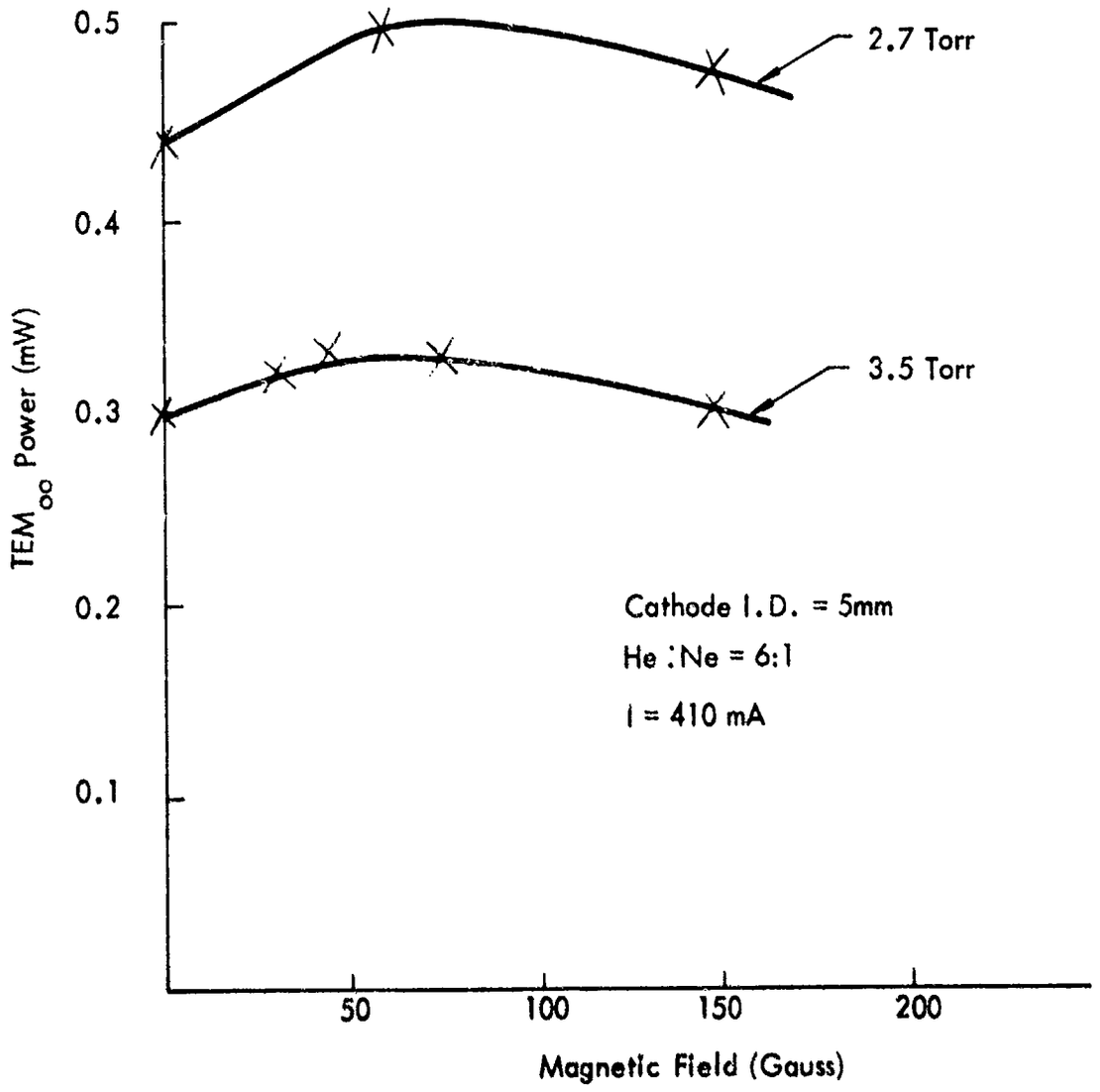

FIGURE 21
LASER POWER VS AXIAL MAGNETIC FIELD - #2 ELECTRODES

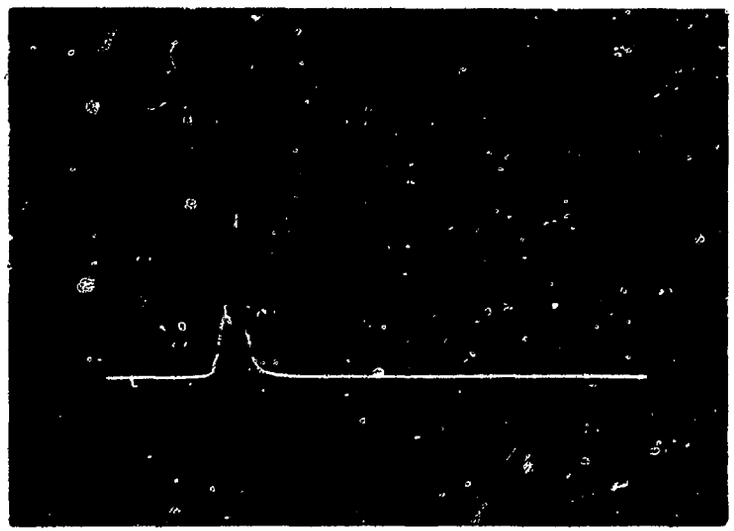

a) Stimulated emission mode spectrum.
Interferometer mirror separation = 1.19 cm.

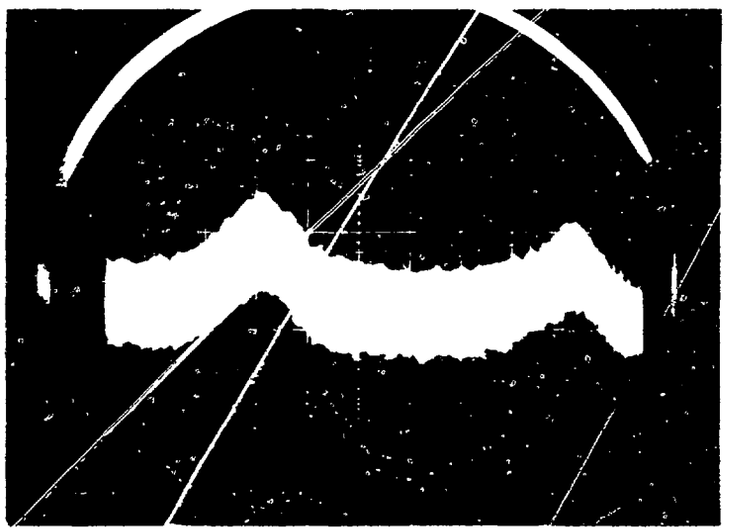

b) Spontaneous emission line width.
Interferometer mirror separation = 0.5 cm.

FIGURE 22
FABRY-PEROT SCANNING INTERFEROMETER TRACINGS.
#3a Electrodes

$$\Delta \sigma_{FS} = 1/(2nd) = \lambda 2/(2nd) = 1 \text{ cm}^{-1} \text{ or } 0.168\text{Å}$$

where n(= 1) is the refractive index of air. The half power width of the display is

$$df = cd\lambda/\lambda^2 = 65 \text{ MHz}$$

As seen in the photograph, the laser was operating on at least two axial modes.

To obtain the spontaneous emission line shape, shown in Figure 22b, the photomultiplier was used to detect the reduced radiance signal. Though filtered with a 50Å wide stop band filter cented at 5328Å a high noise-to-signal ratio is evident. The interferometer spacing was 0.5 cm corresponding to an estimated full-width at half power line of 500 MHz. This high uncertainty value is consistent with the value expected for a doppler broadened 5328Å line at gas temperatures of $\sim 600^{\circ}$K.

5.7 Spectral Noise Characteristics

A Tektronics Model 1L5 spectrum analyzer was employed to measure the power spectrum of optical noise. A typical linear response trace is shown in Figure 23.

The shape of the spectrum (ignoring the instrumental artifacts) corresponds rather closely to that published by Haus, etal[9] for a D. C. excited axial-plasma He-Ne laser. Both APL and HCL lasers show a relatively large amount of noise in the frequency range between 0 and 100 kHz. Spikes in the spectrum which might be caused by axial-mode beats could not be distinguished.

5.8 Minimum Noise Excitation Conditions

A simple power output-vs-time variation of the HCL was observed on an oscilloscope for the #2 electrode set. The detector was arranged to monitor the dependence of laser-light-amplitude fluctuations on excitation conditions. The major fluctuation components includes power supply ripple and an apparent vibration-induced component at 5 kHz caused by the mechanical vacuum pump as coupled into the apparatus. No anomolous amplitude instabilities were observed as excitation conditions were varied. The fluctuation level dropped with increasing output power whether caused by pressure and current changes. All fluctuation components increase drastically as lasing threshold was approached.

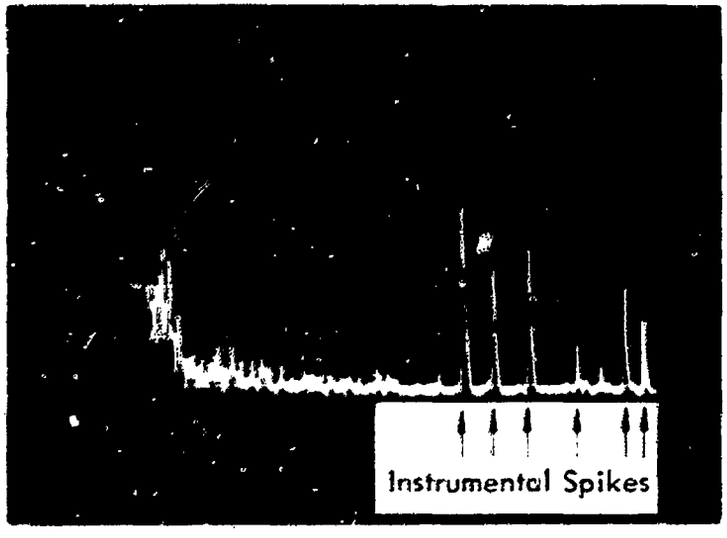

Center frequency = 500 KHz; Dispersion = 100 KHz/cm
Output power = 1.2 mW.

FIGURE 23
NOISE SPECTRUM - #3a ELECTRODES

VI THEORETICAL MODEL, SCALING RELATIONS, AND COMPARISON WITH EXPERIMENT

The primary objective of this section is to derive at an expression, corresponding to Eq. 2-3, to relate the maximum 6328Å gain per unit length, (available from a given HCL) with a fixed slot width to cathode I. D. ratio) to the internal diameter of the cathode. Once substantiated, the relations will be used in the expressions (eqs. 2, 2-7 and 2.2-6) to compute power output and optimal coupling versus gain. This expression is then incorporated in a computer code. The result can be extrapolated and applied to the performance of a 6328Å slotted hollow-cathode laser. The model is derived from application of similarity principles to the cathode region. A qualitative expression for the optimum operating pressure versus cathode I.D., analogous to Eq. 2.1-3, is also obtained from this model. The results are used to interpret the influence of current density, gas-mixture ratio, cathode-slot width, and the behavior of the small (I.D. $\geq$2.5 mm) cathodes.

6.1 Scaling Relation for Optimal HCL Gas Pressure and Laser Gain

The scaling relation assumes a steady-state. The rate equation presumes the upper state population density N_u to depend upon the various plasma parameters.

To first order:

$$\text{Gain} \propto N_u \propto p N_e f \qquad (6.1\text{-}1)$$

where p is the pressure, N_e is the electron density and f depends on the energy distribution of the electrons.

Two features distinguish the negative-glow plasma of an HCL and the positive-column plasma of an APL. First, as the negative glow is a field free region. The discharge current in the negative-glow region is carried by electron diffusion:

$$j_e = N_e V_{diff} \qquad (6.1\text{-}2)$$

where V_{diff} is the average, directed, diffusion velocity of the electrons. However, like the electron drfit velocity of a positive column, the diffusion speed of the negative-glow electrons will be a function of (pD):

$$V_{diff} = \frac{D_e}{p} \frac{1}{N_e} \frac{dN_e}{dx} = V_{diff}(pD) \qquad (6.1\text{-}3)$$

Where D_e is an electron-diffusion coefficient, x is the transverse coordinate, and D is the cathode I.D. As in the positive column, a much

more sensitive dependence on (pD), through the function f, may be anticipated. The gain can be written approximately as:

$$g \propto p j_e f \qquad (6.1\text{-}4)$$

A second important difference between HCL and APL plasma properties relates to the electron energy distribution. The latter is not Maxwellian in the negative glow. Instead, the electrons fall into three groups:[10] the Primary Group - electrons emitted from the cathode, the Secondary Group - ejected electrons resulting from ionization by the primary group, and the Ultimate Group - electrons thermalized to a Maxwellian distribution that behave like positive-column electrons. Only the Secondary and Ultimate Group - electrons contribute significantly to excitation. It is not clear which predominates in laser excitation in a hollow-cathode negative-glow plasma. It has been shown[8], however, that in either case, the excitation function, f, in Eq. (6.1-4) will vary, (as in the positive column case) sensitively with the product (pD). It is not unreasonable to anticipate the existence of a simple pressure-distance product relationship that will maximize at a well defined value of pD. This maximum represents, as in the positive column case, an equilibrium between electron energy distribution and concentration of atoms available for excitation. It is observed experimentally in the hollow-cathode laser, however, that as the pressure is reduced (for a given D) the discharge always becomes unstable (see Figures 11 and 14) before a maximum gain is attained. It is conjectured that this instability will occur whenever the radial dimension of the negative glow become comparable to the I. D. of the cathode. At a pressure corresponding to this condition further decreases in pressure would tend to expell the plasma from the interior of the cathode and cause an abrupt increase in total plasma voltage. At least the hypothesis agrees with experimental observations of visible plasma displacement. It may not be coincidence that the lower limit to pD is close to both measured and calculated[9] values of pt_g (where t_g is the thickness of the negative glow).

The value of the pressure defined by discharge instability in a

He-Ne HCL corresponds to the maximum observed gain. Unlike the positive column discharge, the optimal value for pD cannot be a constant. The thickness of the negative glow, which is equal to the range of the primary electrons through the gas, depends almost linearily upon cathode-potential fall. If one assumes, at the point of instability, that $p\,t_g = pD$, then

$$(pD)_{opt} \propto V_c \tag{6.1-5}$$

where V_c is the cathode-potential fall.

To derive an expression for the dependence of optimum gain on cathode diameter the form of f(pD) must be known. A form approximately consistent with experimental resolution is

$$f(pD) \propto 1/(pD)^2 \tag{6.1-6}$$

At a given current density, using Eqs. (6.1-4), (6.1-5) and (6.1-6), the maximum gain becomes,

$$g_{max} \propto p \cdot \left(\frac{1}{(pD)_{opt}}\right)^2 \tag{6.1-7}$$

$$\propto \frac{1}{V_c D} \tag{6.1-8}$$

From Von Engle's theory[1],

$$j/p^2 \propto V_c^{3/2} \left(1 - V_e/V_c\right)^{5/2} \tag{6.1-9}$$

where j is the total current density at the cathode and $V_e \approx 50$ volts for helium. Note that j and j_e are used interchangeably as the total discharge current in the negative glow is carried by the electrons. Equation 6.1-9, expressed in terms of D at optimal pressure, Eq. (6.1-5) becomes

$$jD^2 \propto V_c^{7/2} \left(1 - V_e/V_c\right)^{5/2} \tag{6.1-10}$$

An expression not inconsistent with the large spread in experimental data is:

$$jD^2 \propto V_c^4 \tag{6.1-11}$$

At constant current density, g_{max} reduces to

$$g_{max} \propto 1/D^{3/2} \tag{6.1-12}$$

Combining Eq. (6.1-5) with Eq. (6.1-11)

Only the form of the equation can be deduced by this very general argument The proportionality constants must be supplied by empirical data obtained from gain measurements at optimal pressure and current. Though the data has more spread than desired some degree of fit to the data yields:

$$g_{max} = 0.7/D^{3/2}\% \text{ per meter} \qquad (6.1\text{-}14)$$

at

$$p\,D^{1/2} \sim 2 \text{ Torr cm}^{1/2} \qquad (6.1\text{-}15)$$

where D is in cm.

Figure 5-12 shows a force fit of formulas (6.1-14) and (6.1-15) to the spread in experimental measurements.

Critical to the above analysis is the assumption of a fixed ratio of slot width to cathode I. D. The analysis and values included in the equations assumes that both the current density and He:NE mixture ratio are held at their respective optimal values.

6.1.1 Optimal Current Density

Optimal current density is observed to be 6 mA/cm^2. This relative low value (compared to the positive column laser ~150 mA/cm^2) is consistent with the higher electron densities in the negative glow. Lower current density is caused by the smaller diffusion-driven drift electron velocity as compared with the field-driven velocity of a positive column.

6.1.2 Optimal Mixture Ratio

An optimum He;Ne mixture ratio was found to be near 20:1 for the 6328Å HCL (see Figures 16 and 18). The difference between this value and the 6:1 value for an optimal He:Ne APL is of interest. As a result of discharge instability, the HCL operates in a relatively high pressure regime. At high pressures the average electron energy is lower. The function, f, in Eq. (6.1-1) can be expected to be more sensitive to the electron-cooling influence of neon. Thus higher He:Ne ratios may be expected.

6.1.3 Slot Width

A comparison of the characteristics of the two 3.5 mm I. D. cathodes, one with a ~40 percent slot width and the other with a ~90

percent slot width (Figures 13 and 14) show higher operating voltage higher optimum pressure, and reduced output power are associated with a wider slot. Higher plasma voltage is caused by reduced negative-glow overlap. As higher plasma voltage increases the thickness of the negative glow,a higher operating pressure is required. Reduced maximum output power is observed (see Eqs. (6.1-5) and (6.1-8).

The difference in performance between the homogeneous discharge distribution,as in the 90 percent cathode slot, and the observed discharge inhomogeneity of the 40 percent slot, is projected to be a function of the Crookes layer requirements. The plasma observed in the tube with 40 percent slot is comparable in thickness of the Crookes layer under operating conditions. An increase from a 40 to 90 percent slot width causes an increase in the electric field of the Crookes layer. The increased field effectively prevents the relatively low energy electrons of the negative glow from passing uniformly through the slot to the anode. At 90 percent slot width the negative glow passes uniformly through the slot.

When Crookes layer blockage occurs in the smaller slot the plasma equilibrates by locally reducing the thickness of the Crookes layer. At a given total current the Crookes layer can contract (laterally) by locally increasing the current density. A longitudinal concentration of the constrained discharge develops, increases the current density, and reduces the Crookes layer thickness to that needed to permit low energy electrons to flow to the anode. This plasma contraction requires only a small increase in cathode fall (compared with a very large increase associated with expulsion of the discharge from the cathode interior). Concentration of the discharge in the small spots, uniformly distributed along the narrow slot, is consistent with minimum energy principles. The near periodic spacing of the spots is doubtless controlled by an equilibrium that develops between space-charge repulsion and the magnetic attraction of parallel current filaments observed by "anode spots". Variation

in the spacing and number of the spots with discharge conditions has been observed to resemble the behavior of anode spots. As gas pressure is reduced, for example, the number of spots reduces and their spacing increases.

For a given cathode I. D., optimum gain is obtained with small slot widths. The above explanation of spot formation indicates the onset of complete negative glow overlap. Formation of cathode spots occurs when the active plasma contracts to the cathode. As considerable cathode errosion occurs when a slot width is chosen close to the point where spots form, a slightly wider slot should be regarded as optimal for longer tube life.

6.1.4 Range of Validity of the Model

An upper limit to cathode I. D. at which formulas (6.1-14) and (6.1-15) fail, is undefined. At some cathode diameter the optimal gain becomes impractically small.

Small cathode diameters lead to two discharge constraints. The cathode voltage for optimal current density decreases with cathode inside diameter. A limiting minimum value that can be obtained, that needed to sustain the discharge, is the normal cathode fall. While the thickness of the negative glow scales with the cathode diameter, the relative thickness of the Crookes region with respect to the negative glow increases (as cathode I. D. is reduced). These constraints produce the unstable discharge conditions observed with the small (1.6 and 2.3 mm I. D.) cathodes. It is inferred that the plasma voltage is considerably higher than the normal cathode fall (by visual estimation of the change in thickness of the Crookes layer).

The Crookes layer and negative glow thicknesses t_c, and t_g vary, at fixed current density, according to[1]:

$$p\, t_g \propto V_c \qquad (6.1\text{-}16)$$

$$p\, t_c \propto \frac{1}{(1 - 50/V_c)} \qquad (6.1\text{-}17)$$

or

$$t_c / t_g = \frac{\text{const.}}{V_c (1 \quad 50/V_c)} \qquad (6.1\text{-}18)$$

A visual examination of the plasma is used to infer that t_c/t_g is close to one for the 3.5 mm I. D. cathode under optimal conditions (p = 4 Torr, V_c = 200 volts), i.e. in Eq. (6.1-18) const. ≈100 volts. As smaller diameter cathodes, e.g. one half this I. D. show intense spatial and temporal fluctuations, a cathode I. D. near 3 mm is probably close to the minimum for optimal performance.

6.2 Slotted Hollow-Cathode-Laser Computer Model

A user-interactive, EXTENDED BASIC computer program, named HCL, is presented in Appendix IV. HCL is completely analogous to the APL program of Appendix II, and serves as a convenient aid for the design of a 6328Å slotted hollow-cathode laser of 40 percent slot width. It only differs from the APL program through the substitution of Eq. (6.1-14) in place of Eq. (2.1-5).

VII THE OPTIMAL SLOTTED HOLLOW-CATHODE LASER

A photograph and schematic illustration of the optimized HCL, as constructed for final comparison measurements with the optimized APL, is shown in Figures 24 and 25 respectively.

The anode and cathode internal diameters, cathode wall thickness, and slot width are identical to those of electrode set #3a of Table I. The cathode and anode lengths are 80 cm and 73 cm respectively. To avoid severe sputtering onto the ceramic insulators, the slot was stopped 2" from each end. The 5 cm long glass-end sections were found to be necessary to avoid contamination of the brewster windows by the low-pressure plasma-expulsion instability. A single boron nitride sleeve was placed near the center of the tube to reduce cathode warping. Unconstrained longitudinal thermal expansion of the cathode is allowed via a slide fit of the cathode in one of the ceramic end sections.

The cavity mirrors could not be mounted directly onto the tubes as severe thermal warping of the tube and cavity misalignment results from asymmetric heating of the thin outer-wall metal jacket. An external framework was constructed to mount the mirrors and plasma tube. Mirror support was provided by three 1-meter long, 3/4" diameter invar rods. Invar was chosen to minimize thermal drift of mirror alignment caused by radiative heat transfer from the plasma tube. The mirror mounts are angularly adjustable about two perpendicular axes. The folded confocal optical cavity configuration consist of a .04 percent transmission flat reflector, and a 0.4 percent transmission, 2 meter radius spherical output reflector.

The final parameters of the optimized HCL tube at seal off were:

Plasma Voltage:	260 VDC
Plasma Current	395 mA
Total Pressure:	6 Torr
Mixture ratio, He:Ne	19:1
TEM_{oo} mode power output:	0.9 ± 0.1 mW

FIGURE 24
PHOTOGRAPH OF OTIMIZED SLOTTED HOLLOW-CATHODE LASER

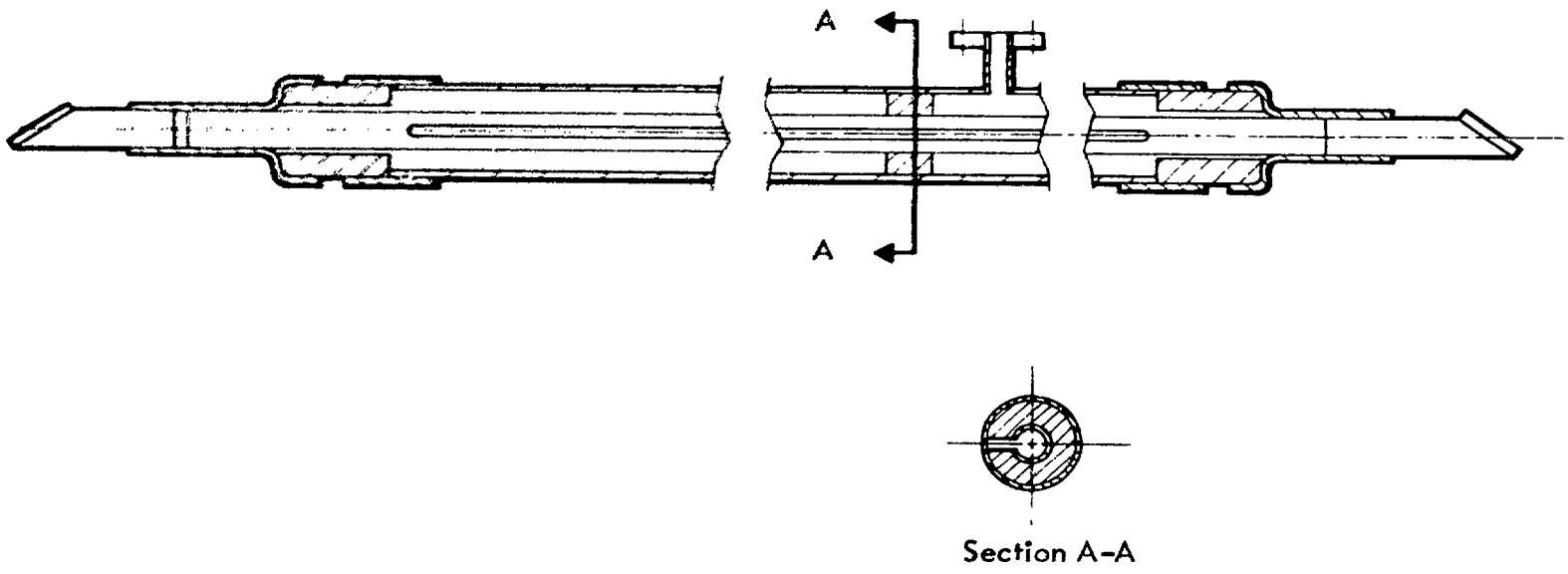

FIGURE 25
SCHEMATIC ILLUSTRATION OF OPTIMIZED SLOTTED HOLLOW-CATHODE LASER

VIII PERFORMANCE COMPARISONS BETWEEN THE OPTIMIZED HOLLOW-CATHODE AND AXIAL PLASMA LASERS

8.1 TEM_{oo} Mode Power Output and Comparative Excitation Characteristics

Optimal TEM_{oo} output power vs. total pressure and discharge current for the optimal APL and HCL are shown in Figures 26 and 27 respectively. Output coupling and He:Ne mixture ratio are set at their respective optimal values for each laser as indicated in the upper right hand portion of the figures.

8.2 Efficiency

The tube voltage at maximum output is also presented in Figures 26 and 27. The net efficiency is calculated by dividing the maximum TEM_{oo} output power by the product of discharge current times tube voltage and is also shown in the figures.

The lower efficiency of the HCL is due in large measure to the inability to reach lower operating pressures in the HCL but may also be due, in part, to the known greater degree of heat generation which occurs in the cathode region relative to the positive column.

8.3 Gain

The maximum gain in the axial plasma laser could not be measured with the single, variable-angle brewster flat used for the gain measurements on the HCL. The large APL gain and small aperture caused unacceptable beam displacement when the flat was set at the angle required to quench oscillation. A gain coefficient of 12 percent per meter is calculated from equation 2.1-5 and is consistent with the observed by varying output mirror transparency and comparing results with equation 2.2-6.

The measured maximum gain of the optimal HCL 2.8 is per cent per meter.

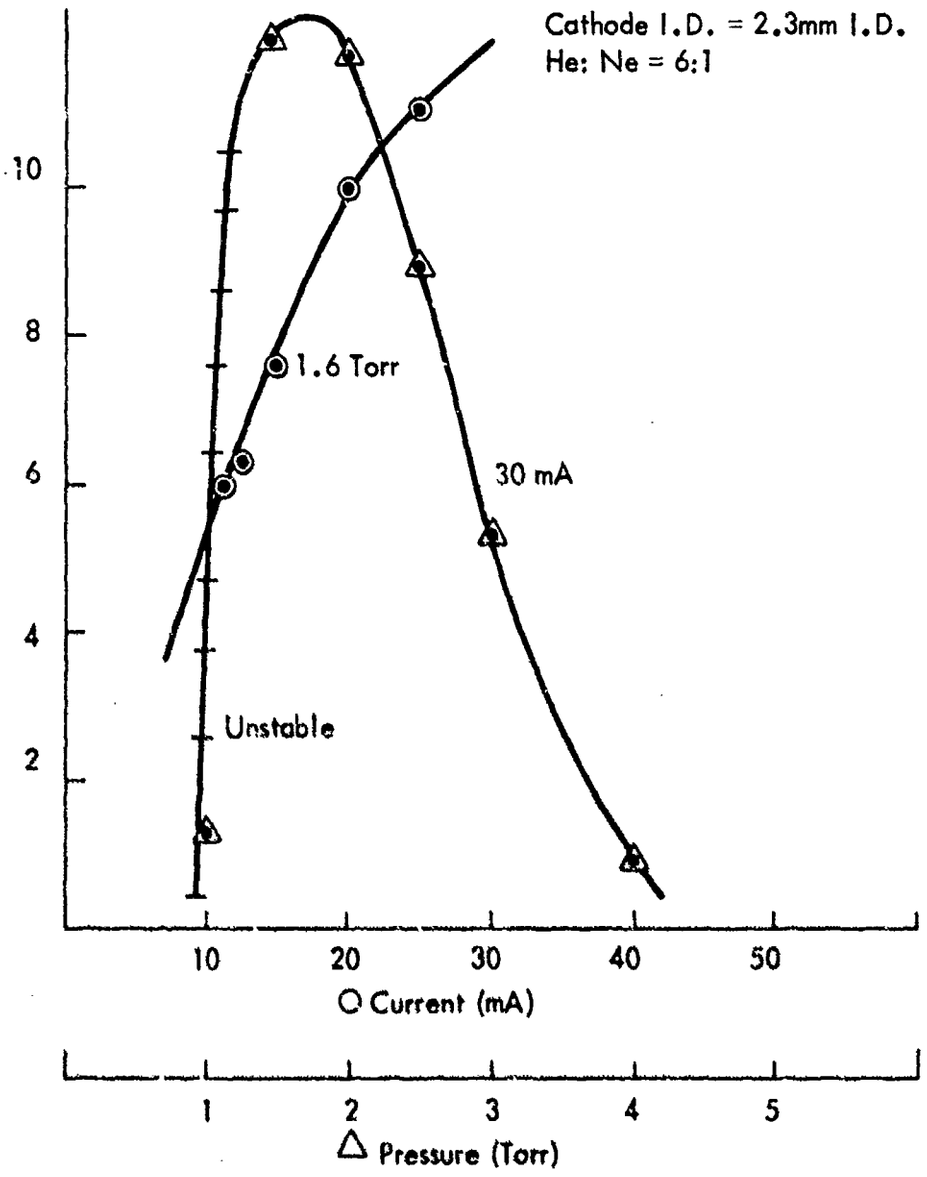

FIGURE 26
TEM_{oo} POWER VS. TOTAL PRESSURE AND DISCHARGE CURRENT-APL

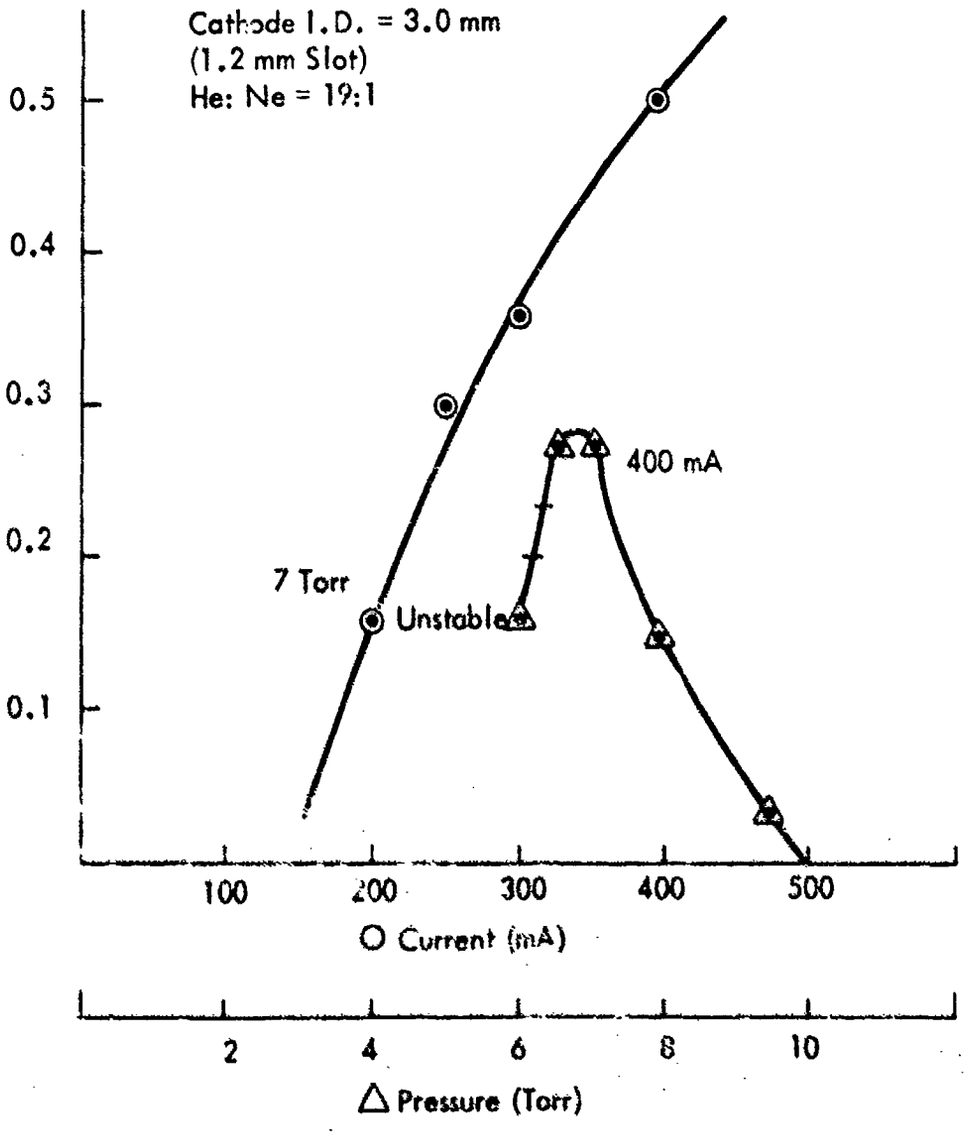

FIGURE 27
TEM_{oo} POWER VS. TOTAL PRESSURE AND DISCHARGE CURRENT-HCL

8.4 Linewidth

Figure 28 compares the spontaneous emission linewidths for the two lasers. Again no significant difference is observable, reflecting evident comparable gas temperatures for the two lasers.

8.5 Relative Axial and Lateral Coherence

8.5.1 Axial Coherence

A direct measure of the axial coherence of the lasers was accomplished by the measurement of the fringe visibility of the interference fringes resulting from the passage of the beam through a Michelson interferometer for various path differences. The fringe visibility, V, is defined by

$$V = \frac{I_{max} - I_{min}}{I_{max} + I_{min}} \qquad (8\text{-}1)$$

where I_{max} and I_{min} refer to the intensity at adjacent maxima and minima of the fringe pattern. V is plotted against path difference in Figure 29 and 30 for the optimized APL and HCL respectively. As expected, V is a damped periodic function of path difference. The "period" corresponds to the beat frequency between axial modes most widely separated in frequency.

8.5.2 Transverse Coherence

A direct measure of the transverse coherence is obtained by measuring the fringe visibility of the interference fringes resulting from the beams passage through a double slit for various slit separations. This data is presented in Figures 31 for both APL and HCL lasers. As expected, the fringe visibility is equal to one within experimental error for slit separations up to the aperture size of the laser. The transverse coherence length of both the APL and

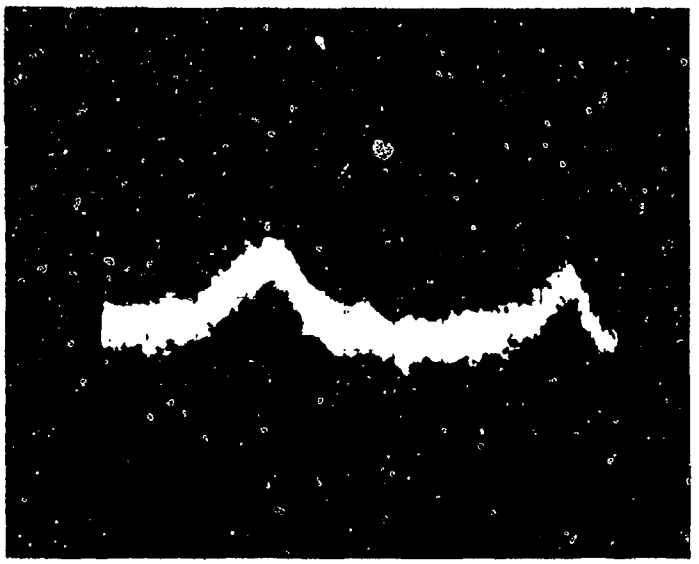

FIGURE 28 (a)
SPONTANEOUS EMISSION LINEWIDTH OF AXIAL PLASMA LASER. d = 0.5 cm.

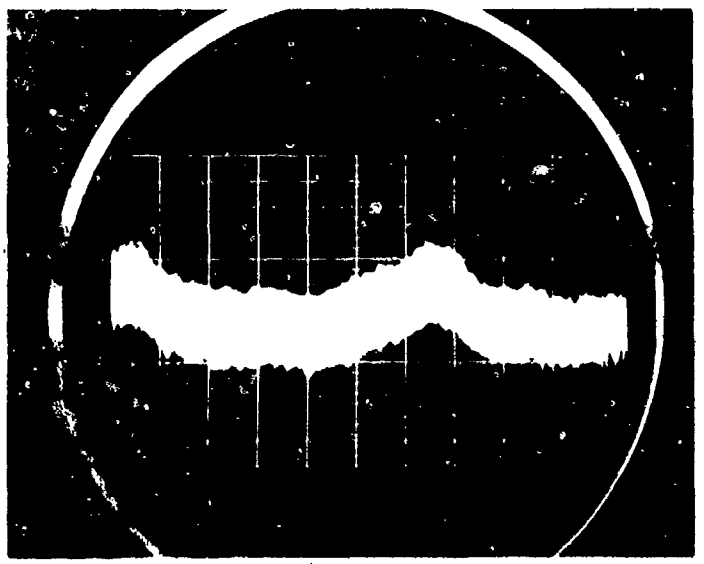

FIGURE 28 (b)
SPONTANEOUS EMISSION LINEWIDTH OF A HOLLOW-CATHODE LASER. d = 0.5 cm.

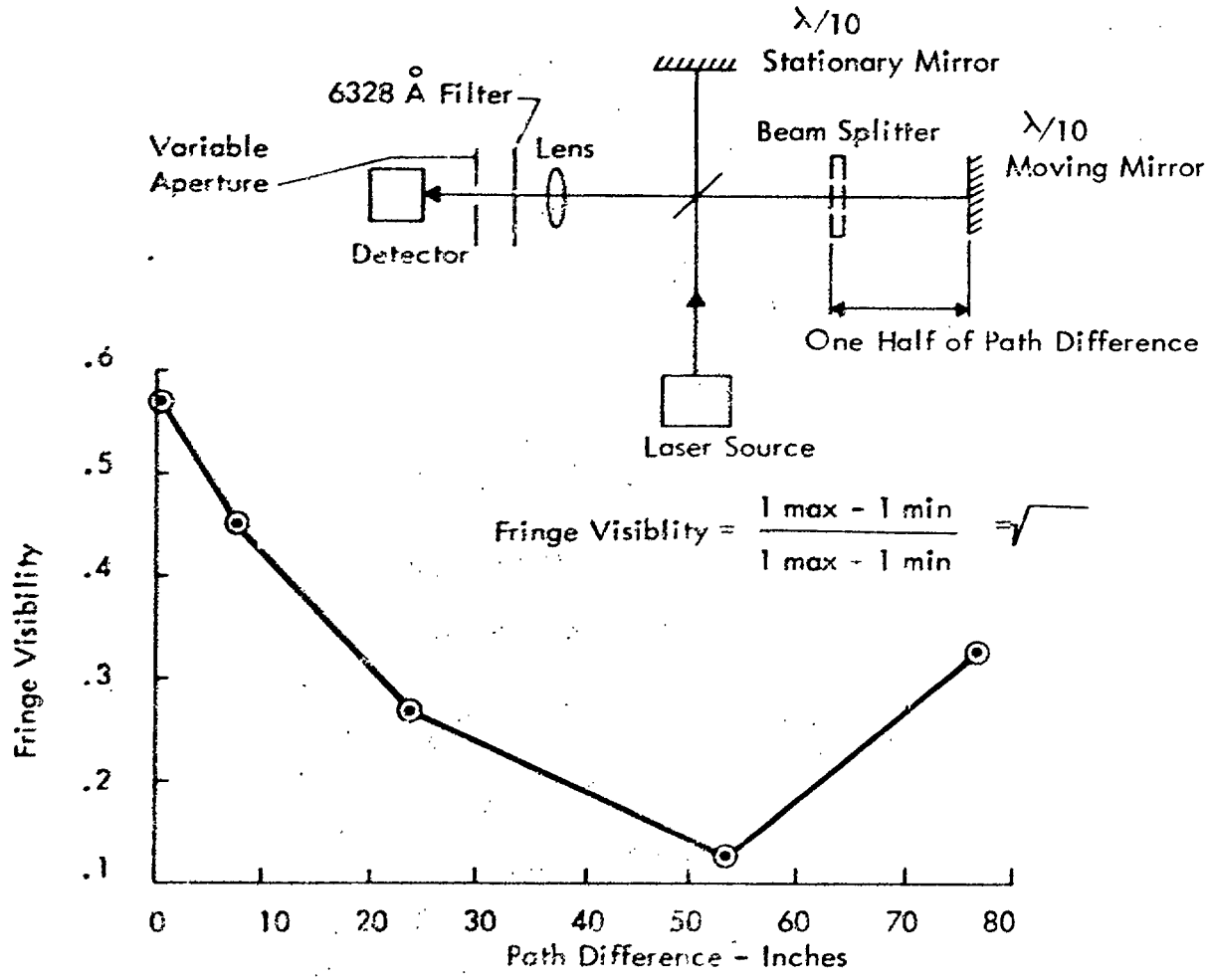

FIGURE 29
FRINGE VISIBILITY VERSUS PATH DIFFERENCE FOR AN APL IN A MICHELSON INTERFEROMETER

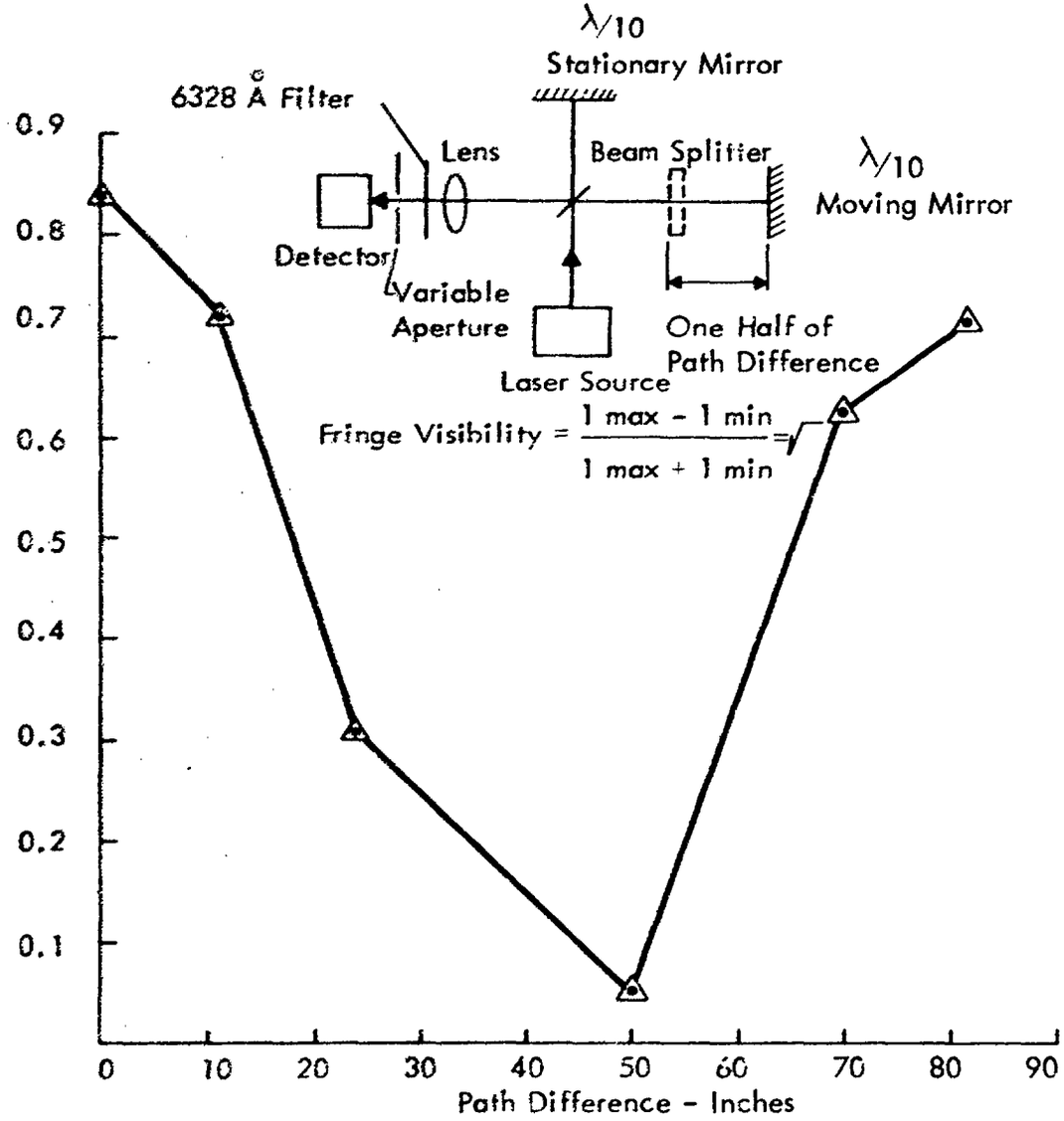

FIGURE 30
FRINGE VISIBILITY VS. PATH DIFFERENCE FOR AN HCL IN A MICHELSON INTERFEROMETER

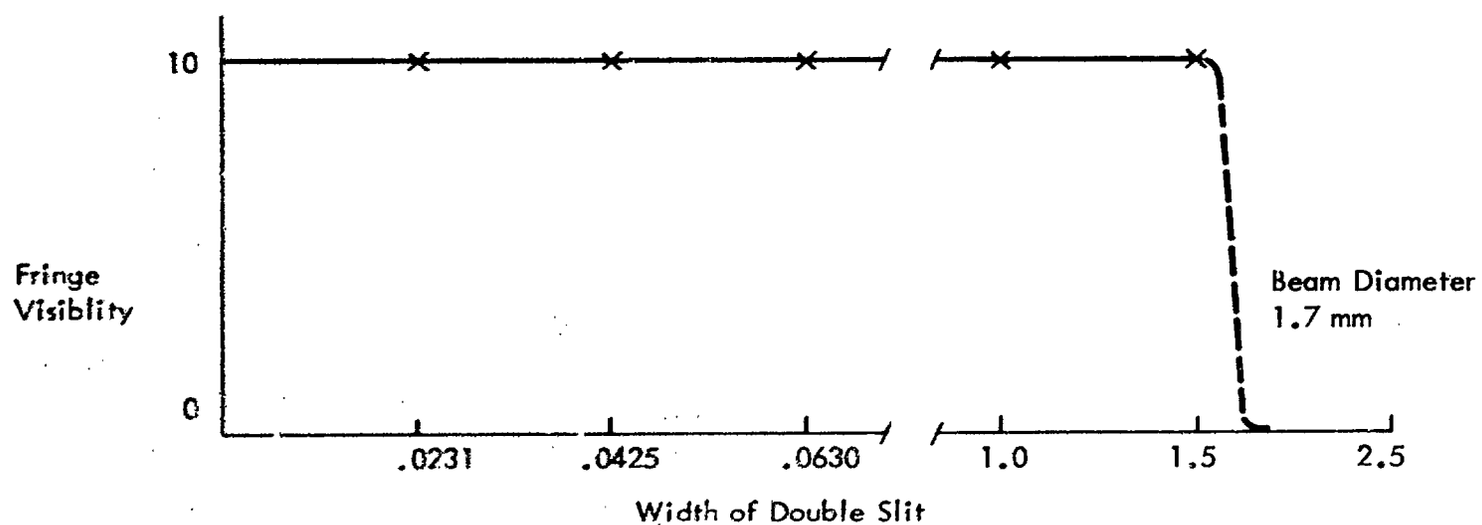

FIGURE 31
LATERAL COHERENCE LENGTH FRINGE VISIBLITY VS. SLIT SEPARATION FOR A DOUBLE-SLIT INTERFERENCE PATTERN-HCL AND APL LASERS ARE INDISTINGUISHABLE

HCL beams is at least equal to the beam diameter.

8.6 Beam Divergence and Spot Size

Measured beam divergence and spot size for the APL and HCL are presented in Table III. The measurements are consistent with what one expects for a TEM_{oo} mode beam in a 1-meter long folded confocal 6328Å laser resonator.

8.7 Angular Drift in Spot Position

The angular position drift of the HCL and APL lasers was measured with a Schottky barrier type photo cell incorporated in ratiometeric differential amplifiers to read x and y beam displacements from a reference zero in the normal plane. Because of the large amount of data needed the amplifiers were fed to 5-1/2 digit digital voltmeter and thence to a minicomputer and magnetic tape recorder. The computer extracted the statistical values from the raw data and summarized the principle results reported herein in block form.

The ratiometric differential amplifers were first zero checked by reading a high intensity frosted bulb tungsten-filament lamp for 3777 samples. Data were taken for maximum, minimum, average, and standard deviation values from an electrically set zero. The measurement system sensitivity was set to 97.1 microradians/volt.

Table IV summarizes the extreme stability and accuracy of the zero setting that was obtained in a quiet laboratory during an overnight run. The interpretation of symbolism is as follows:

X, Y = ± deviation of the electrical from the mechanical zero. Values of the corresponding variables are output on a cumulative basis. Units are milliradians referred to a source 468 inches from the detector.

XT, YT = ± deviation in X and Y as incrementally reported every 1000th data sample or at the termination of a run. Thus data for 1000, 2000, 3000, 3777 samples are output for 1000th sample increments and one 777th sample increment. Units are milliradians.

TABLE III
BEAM DIVERGENCE AND SPOT SIZE

LASER	TEM_{oo} Spot Size (cm)	TEM_{oo} Beam Divergence (m rad.)
APL	$0.169 \pm .003$	$0.475 \pm .008$
HCL	$0.149 \pm .003$	$0.539 \pm .008$

TABLE IV
ZERO DRIFT STABILITY TESTS OF PRECISION
RATIOMETRIC POSITION DETECTOR
468" REFERENCE DISTANCE

```
FNF--TNF
INPUT CONSTANT IN MILLIRADIANS PER VOLT    .0971
INPUT FILE NAME    MT0:1
```

	MU	SIGMA	MAX	MIN	# SAMPLES
X	-0.0159	0.00011	-0.0154	-0.0161	1000.
XT	-0.0159	0.00011	-0.0154	-0.0161	1000.
Y	-0.0103	0.00002	-0.0103	-0.0104	1000.
YT	-0.0103	0.00002	-0.0103	-0.0104	1000.
R	0.0000	0.00006	0.0005	0.0000	1000.
RT	0.0000	0.00006	0.0005	0.0000	1000.

	MU	SIGMA	MAX	MIN	# SAMPLES
X	-0.0159	0.00011	-0.0154	-0.0163	2000.
XT	-0.0160	0.00008	-0.0157	-0.0163	1000.
Y	-0.0103	0.00003	-0.0102	-0.0104	2000.
YT	-0.0103	0.00002	-0.0102	-0.0104	1000.
R	0.0000	0.00006	0.0005	0.0000	2000.
RT	0.0000	0.00005	0.0003	0.0000	1000.

	MU	SIGMA	MAX	MIN	# SAMPLES
X	-0.0159	0.00010	-0.0154	-0.0163	3000.
XT	-0.0159	0.00008	-0.0156	-0.0161	1000.
Y	-0.0103	0.00003	-0.0102	-0.0104	3000.
YT	-0.0103	0.00001	-0.0102	-0.0103	1000.
R	0.0000	0.00005	0.0005	0.0000	3000.
RT	0.0000	0.00005	0.0003	0.0000	1000.

	MU	SIGMA	MAX	MIN	# SAMPLES
X	-0.0159	0.00009	-0.0154	-0.0163	3777.
XT	-0.0159	0.00008	-0.0156	-0.0161	777.
Y	-0.0103	0.00004	-0.0102	-0.0104	3777.
YT	-0.0102	0.00001	-0.0102	-0.0103	777.
R	0.0000	0.00005	0.0005	0.0000	3777.
RT	0.0000	0.00005	0.0003	0.0000	777.

```
STOP 1
R
```

MBA

R, RT = ± are the radial deviation of a vector in the X-Y plane expressed as an angle and referred to a source 468 inches from the detector. Units are milliradians.

The results of the zero stability tests indicate that errors in beam pointing as small as 100 nanoradians can be measured with confidence.

Table V summarizes the results of 4339 samples of angular drift for the optimized HCL laser. There appears to be a gradual drift in the X-direction of almost 1.97 microradians where as the Y-direction drift is only 70 nanoradians during the same interval. The X-drift corresponds to a net motion of approximately 0.001" in 40 ft. The difference between the X and Y drift values is perhaps due to localized heating of the Invar rods by the hot side of the HCL tube.

Table VI summarizes the results of 12,000 samples of angular drift for the APL laser. Because the optical cavity was open and heating could warp the mirror holders in the vertical plane, Y drift is anticipated whereas X drift should be small. The changes in X and Y over the prolonged run show $\Delta X = 1.8$ microradian and $\Delta Y < 0.1$ microradian.

Comparing the sigma values for HCL and APL laser for approximately 4000 samples one can conclude that:

a) The absolute values for the drifts are of the order of 1 microradian.

b) There tends to be more drift in one direction as compared with its orthogonal coordinate.

c) The relative drift of the HCL laser cavity is greater than the APL cavity, though the absolute drift is still exceedingly small. Because of the small values involved it seems reasonable to conclude that the differences in angular drift are more a property of the optical cavity geometry than whether the optical cavity is excited by an axial plasma or slotted hollow-cathode plasma tube.

TABLE V
ANGULAR DRIFT OF AN HCL BEAM
490" REFERENCE DISTANCE

```
FTNF
INPUT CONSTANT IN MILLIRADIANS PER VOLT    .0928
INPUT FILE NAME    MT0:0
          MU        SIGMA       MAX         MIN       # SAMPLES
X       -0.0875     0.00193    -0.0812     -0.0934      1000.
XT      -0.0875     0.00193    -0.0812     -0.0934      1000.
Y        0.0588     0.00218     0.0665      0.0531      1000.
YT       0.0588     0.00218     0.0665      0.0531      1000.
R        0.0026     0.00140     0.0082      0.0000      1000.
RT       0.0026     0.00140     0.0082      0.0000      1000.


          MU        SIGMA       MAX         MIN       # SAMPLES
X       -0.0862     0.00224    -0.0776     -0.0934      2000.
XT      -0.0850     0.00177    -0.0776     -0.0905      1000.
Y        0.0588     0.00213     0.0665      0.0529      2000.
YT       0.0588     0.00208     0.0651      0.0529      1000.
R        0.0026     0.00141     0.0106      0.0000      2000.
RT       0.0024     0.00129     0.0095      0.0001      1000.


          MU        SIGMA       MAX         MIN       # SAMPLES
X       -0.0850     0.00271    -0.0766     -0.0934      3000.
XT      -0.0826     0.00177    -0.0766     -0.0872      1000.
Y        0.0585     0.00220     0.0666      0.0520      3000.
YT       0.0580     0.00222     0.0666      0.0520      1000.
R        0.0029     0.00153     0.0106      0.0000      3000.
RT       0.0025     0.00136     0.0088      0.0000      1000.


          MU        SIGMA       MAX         MIN       # SAMPLES
X       -0.0838     0.00319    -0.0745     -0.0934      4000.
XT      -0.0804     0.00156    -0.0745     -0.0862      1000.
Y        0.0582     0.00227     0.0666      0.0492      4000.
YT       0.0570     0.00212     0.0649      0.0492      1000.
R        0.0032     0.00164     0.0115      0.0000      4000.
RT       0.0023     0.00136     0.0085      0.0000      1000.


          MU        SIGMA       MAX         MIN       # SAMPLES
X       -0.0835     0.00330    -0.0745     -0.0934      4339.
XT      -0.0794     0.00139    -0.0748     -0.0824       339.
Y        0.0581     0.00225     0.0666      0.0492      4339.
YT       0.0574     0.00180     0.0625      0.0529       339.
R        0.0033     0.00165     0.0115      0.0000      4339.
RT       0.0020     0.00108     0.0053      0.0001       339.
STOP 1
R
```

TABLE VI
ANGULAR DRIFT OF AN APL BEAM
288" REFERENCE DISTANCE

FTNF
INPUT CONSTANT IN MILLIRADIANS PER VOLT .1578
INPUT FILE NAME MT0:8

	MU	SIGMA	MAX	MIN	# SAMPLES
X	-0.0245	0.00190	-0.0183	-0.0305	1000.
XT	-0.0245	0.00190	-0.0183	-0.0305	1000.
Y	-0.0390	0.00247	-0.0317	-0.0469	1000.
YT	-0.0390	0.00247	-0.0317	-0.0469	1000.
R	0.0028	0.00140	0.0083	0.0000	1000.
RT	0.0028	0.00140	0.0083	0.0000	1000.

	MU	SIGMA	MAX	MIN	# SAMPLES
X	-0.0238	0.00197	-0.0164	-0.0321	2000.
XT	-0.0231	0.00177	-0.0164	-0.0321	1000.
Y	-0.0404	0.00259	-0.0317	-0.0490	2000.
YT	-0.0417	0.00188	-0.0336	-0.0490	1000.
R	0.0027	0.00143	0.0105	0.0000	2000.
RT	0.0021	0.00143	0.0098	0.0000	1000.

	MU	SIGMA	MAX	MIN	# SAMPLES
X	-0.0231	0.00213	-0.0139	-0.0321	3000.
XT	-0.0218	0.00160	-0.0139	-0.0309	1000.
Y	-0.0411	0.00264	-0.0317	-0.0497	3000.
YT	-0.0427	0.00193	-0.0360	-0.0497	1000.
R	0.0028	0.00148	0.0105	0.0000	3000.
RT	0.0022	0.00138	0.0099	0.0000	1000.

	MU	SIGMA	MAX	MIN	# SAMPLES
X	-0.0227	0.00215	-0.0139	-0.0321	4000.
XT	-0.0213	0.00153	-0.0164	-0.0268	1000.
Y	-0.0417	0.00261	-0.0317	-0.0497	4000.
YT	-0.0435	0.00151	-0.0376	-0.0483	1000.
R	0.0028	0.00141	0.0105	0.0000	4000.
RT	0.0015	0.00112	0.0070	0.0000	1000.

	MU	SIGMA	MAX	MIN	# SAMPLES
X	-0.0224	0.00210	-0.0139	-0.0321	5000.
XT	-0.0212	0.00149	-0.0148	-0.0270	1000.
Y	-0.0419	0.00246	-0.0317	-0.0497	5000.
YT	-0.0428	0.00145	-0.0379	-0.0493	1000.
R	0.0027	0.00139	0.0105	0.0000	5000.
RT	0.0018	0.00109	0.0067	0.0000	1000.

	MU	SIGMA	MAX	MIN	# SAMPLES
X	-0.0222	0.00206	-0.0139	-0.0321	6000.
XT	-0.0212	0.00134	-0.0154	-0.0270	1000.
Y	-0.0420	0.00233	-0.0317	-0.0508	6000.
YT	-0.0420	0.00153	-0.0351	-0.0508	1000.
R	0.0026	0.00136	0.0105	0.0000	6000.
RT	0.0017	0.00108	0.0088	0.0000	1000.

TABLE VI (Continued)

	MU	SIGMA	MAX	MIN	# SAMPLES
X	-0.0221	0.00199	-0.0139	-0.0321	7000.
XT	-0.0216	0.00143	-0.0161	-0.0262	1000.
Y	-0.0418	0.00226	-0.0317	-0.0508	7000.
YT	-0.0409	0.00148	-0.0361	-0.0457	1000.
R	0.0025	0.00137	0.0105	0.0000	7000.
RT	0.0018	0.00099	0.0056	0.0000	1000.

	MU	SIGMA	MAX	MIN	# SAMPLES
X	-0.0223	0.00200	-0.0139	-0.0321	8000.
XT	-0.0238	0.00129	-0.0190	-0.0294	1000.
Y	-0.0415	0.00235	-0.0317	-0.0508	8000.
YT	-0.0392	0.00163	-0.0328	-0.0453	1000.
R	0.0026	0.00137	0.0105	0.0000	8000.
RT	0.0018	0.00105	0.0082	0.0000	1000.

	MU	SIGMA	MAX	MIN	# SAMPLES
X	-0.0225	0.00199	-0.0139	-0.0321	9000.
XT	-0.0238	0.00121	-0.0196	-0.0277	1000.
Y	-0.0410	0.00272	-0.0281	-0.0508	9000.
YT	-0.0369	0.00175	-0.0281	-0.0425	1000.
R	0.0028	0.00154	0.0133	0.0000	9000.
RT	0.0018	0.00111	0.0090	0.0000	1000.

	MU	SIGMA	MAX	MIN	# SAMPLES
X	-0.0226	0.00196	-0.0139	-0.0321	10000.
XT	-0.0235	0.00140	-0.0180	-0.0287	1000.
Y	-0.0404	0.00316	-0.0281	-0.0508	10000.
YT	-0.0351	0.00160	-0.0296	-0.0400	1000.
R	0.0031	0.00175	0.0133	0.0000	10000.
RT	0.0019	0.00103	0.0063	0.0001	1000.

	MU	SIGMA	MAX	MIN	# SAMPLES
X	-0.0226	0.00198	-0.0139	-0.0321	11000.
XT	-0.0231	0.00102	-0.0193	-0.0269	1000.
Y	-0.0398	0.00363	-0.0261	-0.0508	11000.
YT	-0.0335	0.00126	-0.0261	-0.0382	1000.
R	0.0034	0.00196	0.0137	0.0000	11000.
RT	0.0014	0.00082	0.0075	0.0000	1000.

	MU	SIGMA	MAX	MIN	# SAMPLES
X	-0.0227	0.00189	-0.0139	-0.0321	12000.
XT	-0.0240	0.00108	-0.0212	-0.0283	1000.
Y	-0.0398	0.00421	-0.0252	-0.0508	12000.
YT	-0.0313	0.00129	-0.0252	-0.0346	1000.
R	0.0038	0.00229	0.0139	0.0000	12000.
RT	0.0015	0.00082	0.0066	0.0000	1000.

9.0 CONCLUSIONS AND RECOMMENDATIONS

The most important deterent to immediate application of a c. w. slotted hollow-cathode laser as a ruggedized high-reliability, low-voltage laser is sputtering and therefore short operating lifetime as a sealed metal-walled laser.

A crucial low pressure instability currently places a constraint on the maximum power output at 6328Å. The tendency of the HCL, when power optimized for 6328Å transition, to operate at lower pressures than the APL necessitates that the HCL operate more efficiently if it is to compete in terms of power. No basis for this ability was found in this research.

The low-power instability was not found for laser transitions pumped by the triplet metastable level (2^3S_1) of helium such as the neon 11523Å line. Preliminary tests on the 11523Å line indicate that c. w. slotted hollow-cathode discharge may outperform the comparable APL laser. Power outputs of up to 30 mW were obtained with mirrors that were not power optimized. At the maximum excitation current used the power slope was still positive. More research is indicated in this area of a higher power compact 11523Å laser source.

Two methods, alternative to reducing the gas pressure, may be investigated to improve HCL average power:

- Operate under pulsed conditions to increase the average electron energy on a transient basis.
- Introducing a grid or similar structure in the plasma upon which electron-ion recombination can occur.
- Neither method can be expected to increase power efficiency by an order of magnitude.

The slot geometry of the discharge profoundly affects the laser efficiency and stability. Further experimentation on other than the slotted hollow cathode geometry would seem appropriate. A perforated cathode with holes of the same relative area as seen in the sputter markings on the cathode slot would be a good starting point.

10.0 REFERENCES

1. Schuebel, W. F. "Conference on Hollow-Cathode Discharges and Their Applications", Orsay, France, Sept. 1971

2. Engel, A. von, Ionized Gases (Oxford University Press, 1965)

3. Pressley, R. J. (Ed.) Handbook of Lasers with Selected Data on Optical Technology, (The Chemical Rubber Co., 1971)

4. Yariv, Amnon, Quantum Electronics (Wiley & Sons, New York, 1967)

5. Smith, P.W., IEEE J. Quant. Elect., QE-2, 62 (1966)

6. Smith, P.W., IEEE J. Quant. Elect., QE-2, 77 (1966)

7. Born M., and Wolf, E., Principles of Optics (Pergamon Press, 1970)

8. Flugge, S., Handbuch der Physik (Springer-Verlag, Berlin, 1965) p. 53

9. Bellisio, J.A., Freed, C. Haus, H. A. Applied Phys. Lett. 4, 5 (1964)

10. Palmer, A. J., Ph.D. Thesis, University of Western Ontario (1971)

APPENDIX I
CAV Computer Program

```
CAV

0010  REM PROG CALCS LASER SPOT SIZE AT THE MIRRORS OF A FOLDED
0020  REM CONFOCAL RESONATOR (W0 & W1) AND SYMETRIC CONFOCAL
0030  REM RESONATOR (W2) AND DIFFRACTION LIMITED TUBE DIAMETER, 4W1
0040  REM AND 4W2 RESPECTIVELY AS A FUNCTION OF MIRROR SEPARATION, D,
0050  REM FOR A WAVELENGTH OF 6329A
0060  DIM D(100)
0070  PRINT "INPUT THE NUMBER OF MIRROR SEPARATIONS TO BE TESTED"
0080  INPUT B
0090  PRINT "INPUT THE VALUES FOR MIRROR SEPERATION IN CM"
0100   FOR J=1 TO B
0110   INPUT D(J)
0115   NEXT J
0120  PRINT
0130  PRINT "**********************************************************************"
0140  PRINT
0150  PRINT "D(CM)";TAB(10);"W0(CM)";TAB(26);"W1(CM)";TAB(41);
0155  PRINT "W2(CM)";TAB(54);"4W1(CM)";TAB(64);"4W2(CM)"
0170  PRINT
0180  PRINT "**********************************************************************"
0190  PRINT
0200   FOR J=1 TO B
0210   W0=(6.328E-05*2*D(J)/(2*3.14))^(1/2)
0220   W1=W0*1.41
0230   W2=W0
0240   W3=4*W1
0250   W4=4*W2
0260   PRINT D(J);W0;W1;W2;W3;W4
0270   NEXT J
0280  END
```

APPENDIX I
CAV COMPUTER PROGRAM

```
RUN
CAV

INPUT THE NUMBER OF MIRROR SEPARATIONS TO BE TESTED
?1
INPUT THE VALUES FOR MIRROR SEPERATION IN C4
?100

*****************************************************************

U(C4)     W0(CM)          W1(CM)          W2(CM)        4W1(C4)   4W2(CM)

*****************************************************************

 100   4.48919E-02    6.32976E-02    4.48914E-02    .253191     .17956

DONE
```

APPENDIX I (Continued)

APPENDIX II
APL Computer Program

APL

```
0010  REM PROG CALCS FOR A 6328A HE-NE APL, MAX GAIN, OPT MIRR TRANS,
0020  REM AND CORRESPDING OPT WATTS/CM##2 OUT, AND MAX WATTS/CM##2
0030  REM FOR OTHER MIRROR TRANSPARENCIES VS PLASMA LENGTH, L, TUBE
0040  REM DIAMETER, D, AND LOSS COEFICIENT, A.
0050  DIM A(100),D(100),L(100),T(100)
0060  PRINT "HOW MANY VALUES OF OUTPUT MIRROR TRANSP WILL BE TESTED?"
0090  INPUT T
0100  PRINT "INPUT THE VALUES FOR TRANSMISSION"
0110   FOR I=1 TO T
0120   INPUT T(I)
0130   NEXT I
0140  PRINT "HOW MANY VALUES OF PLASMA LENGTH WILL BE TESTED?"
0150  INPUT D
0160  PRINT "INPUT THE VALUES OF PLASMA LENGTH IN CM"
0170   FOR J=1 TO D
0180   INPUT L(J)
0190   NEXT J
0260  PRINT "HOW MANY VALUES FOR THE LOSS COEF WILL BE TESTED"
0270  INPUT A
0280  PRINT "INPUT THE VALUES FOR THE LOSS COEFICIENT"
0290   FOR K=1 TO A
0300   INPUT A(K)
0310   NEXT K
0320  PRINT "HOW MANY VALUES FOR TUBE DIAMETER WILL BE TESTED"
0330  INPUT G
0340  PRINT "INPUT THE VALUES FOR TUBE DIAMETER IN CM"
0350   FOR U=1 TO G
0360   INPUT D(U)
0370   NEXT U
0390   FOR J=1 TO D
0400    FOR K=1 TO A
0410     FOR U=1 TO G
0411     G=(.0003/D(U))*L(J)
0412     T0=EXP(A(K)/G)*(1/2)*(1-(A(K)/G)*(1/2))
0413     P0=30*G*(1-(A(K)/G)*(1/2))^2
0420     PRINT
0430     PRINT "**********************************************"
0440     PRINT
0460     PRINT
0470     PRINT "TUBE DIAM = ";D(U);"LOSS COEF =";A(K);"LENGTH =";L(J)
0480     PRINT
0481     PRINT TAB(-18);"GAIN = ";G
0482     PRINT TAB(18);"OPT TRANSMISSION = ";T0
0483     PRINT TAB(18);"OPT WATTS/CM##2 OUT = ";P0
0484     PRINT
0490     PRINT "**********************************"
0500     PRINT
0510     PRINT "TRANSMISSION,T=","WATTS/CM##2 OUT,P="
0520     PRINT
0530      FOR I=1 TO T
0540      P=30*T(I)*(G/(A(K)+T(I))-1)
0560      PRINT T(I),P
0570      NEXT I
0590     NEXT U
0610    NEXT K
0630   NEXT J
0680  END
```

APPENDIX II
APL COMPUTER PROGRAM

```
APL

HOW MANY VALUES OF OUTPUT MIRROR TRANSP WILL BE TESTED?
?5
INPUT THE VALUES FOR TRANSMISSION
?.01
?.025
?.03
?.04
?.05
HOW MANY VALUES OF PLASMA LENGTH WILL BE TESTED?
?1
INPUT THE VALUES OF PLASMA LENGTH IN CM
?100
HOW MANY VALUES FOR THE LOSS COEF WILL BE TESTED
?1
INPUT THE VALUES FOR THE LOSS COEFICIENT
?.005
HOW MANY VALUES FOR TUBE DIAMETER WILL BE TESTED
?1
INPUT THE VALUES FOR TUBE DIAMETER IN CM
?.25

**********************************************


TUBE DIAM = .25       LOSS COEF = .005      LENGTH = 100

               GAIN = .12
               OPT XMISSION = 3.89898E-02
               OPT WATTS/CM**2 OUT = 2.28031

**********************************************

XMISSION,T     WATTS/CM**2 OUT,P

 .01           2.1
 .025          2.25
 .03           2.18571
 .04           2
 .05           1.77273

DONE
```

APPENDIX II (Continued)

APPENDIX III
Gain Measurement Calibration

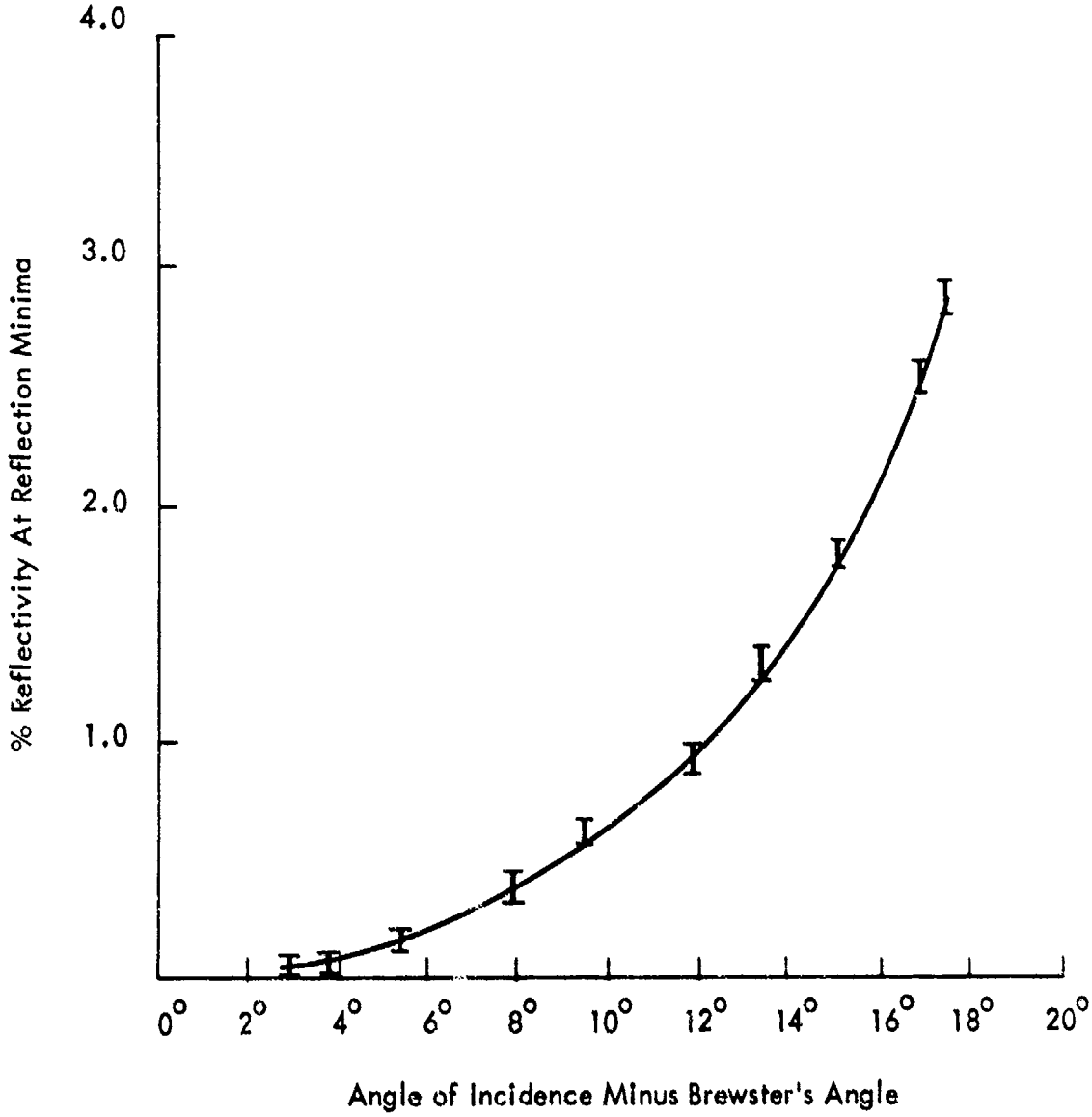

REFLECTIVITY AT REFLECTION MINIMA FROM A 1/2 mm THICK OPTICAL FLAT FOR 6328 A LASER RADIATION POLARIZED PARALLEL TO THE PLANE OF INCIDENCE VS ANGLE OF INCIDENCE

APPENDIX IV
HCL Computer Program

```
HCL

0010  REM PROG CALCS FOR A 6328A HE-NE APL, MAX GAIN, OPT MIRR TRANS,
0020  REM AND CORRESPDING OPT WATTS/CMAR2 OUT, AND MAX WATTS/CMAR2
0030  REM FOR OTHER MIRROR TRANSPARENCIES VS PLASMA LENGTH, L, TUBE
0040  REM DIAMETER, D, AND LOSS COEFICIENT, A.
0050  DIM A(100),D(100),L(100),T(100)
0080  PRINT "HOW MANY VALUES OF OUTPUT MIRROR TRANSP WILL BE TESTED?"
0090  INPUT T
0100  PRINT "INPUT THE VALUES FOR TRANSMISSION"
0110   FOR I=1 TO T
0120   INPUT T(I)
0130   NEXT I
0140  PRINT "HOW MANY VALUES OF PLASMA LENGTH WILL BE TESTED?"
0150  INPUT O
0160  PRINT "INPUT THE VALUES OF PLASMA LENGTH IN CM"
0170   FOR J=1 TO O
0180   INPUT L(J)
0190   NEXT J
0200  PRINT "HOW MANY VALUES FOR THE LOSS COEF WILL BE TESTED"
0210  INPUT A
0220  PRINT "INPUT THE VALUES FOR THE LOSS COEFICIENT"
0230   FOR K=1 TO A
0240   INPUT A(K)
0250   NEXT K
0260  PRINT "HOW MANY VALUES FOR TUBE DIAMETER WILL BE TESTED"
0330  INPUT G
0340  PRINT "INPUT THE VALUES FOR TUBE DIAMETER IN CM"
0350   FOR U=1 TO G
0360   INPUT D(U)
0370   NEXT U
0380   FOR J=1 TO O
0400    FOR K=1 TO A
0410     FOR U=1 TO G
0411     G=(.00007/D(U)*(3/2))^L(J)
0412     T0=2869(A(K)^G)*(1/2)^(1-(A(K)/G)*(1/2))
0413     P0=6946(1-(A(K)/G)*(1/2))^2
0420     PRINT
0430     PRINT "&&&&&&&&&&&&&&&&&&&&&&&&&&&&&&&&&&&&&&&&&&&&&&&&&&&&&&&&"
0440     PRINT
0460     PRINT
0470     PRINT "TUBE DIAM = ";D(U);"LOSS COEF =";A(K);"LENGTH =";L(J)
0480     PRINT
0481     PRINT TAB(10);"GAIN = ";G
0482     PRINT TAB(10);"OPT EMISSION = ";T0
0483     PRINT TAB(10);"OPT WATTS/CMAR2 OUT = ";P0
0484     PRINT
0490     PRINT "&&&&&&&&&&&&&&&&&&&&&&&&&&&&&&&&&&&&&&&&&&&&&&&&&&&&&&&&"
0500     PRINT
0510     PRINT "EMISSION,T=","WATTS/CMAR2 OUT,P="
0520     PRINT
0530      FOR I=1 TO T
0540      P=30*T(I)*(G/(A(K)+(T(I)/2)))^(1/2)-1)
0550      PRINT T(I),P
0570      NEXT I
0580     NEXT U
0610    NEXT K
0630   NEXT J
0640  END
```

APPENDIX IV
HCL COMPUTER PROGRAM

```
RUN
HCL

HOW MANY VALUES OF OUTPUT MIRROR TRANSP WILL BE TESTED?
?4
INPUT THE VALUES FOR TRANSMISSION
?.01
?.02
?.03
?.04
HOW MANY VALUES OF PLASMA LENGTH WILL BE TESTED?
?1
INPUT THE VALUES OF PLASMA LENGTH IN CM
?100
HOW MANY VALUES FOR THE LOSS COEF WILL BE TESTED
?1
INPUT THE VALUES FOR THE LOSS COEFICIENT
?.005
HOW MANY VALUES FOR TUBE DIAMETER WILL BE TESTED
?1
INPUT THE VALUES FOR TUBE DIAMETER IN CM
?.35

**********:**********

TUBE DIAM = .35      LOSS COEF = .005      LENGTH = 100

              GAIN = 3.380626E-02
              OPT XMISSION = 1.60024E-02
              OPT WATTS/CM**2 OUT = .768228

**********:**********

XMISSION,T    WATTS/CM**2 OUT,P

.01           .714185
.02           .752247
.03           .621278
.04           .422696

DONE
```

APPENDIX IV (Continued)

UNCLASSIFIED

Security Classification

DOCUMENT CONTROL DATA - R & D

Security classification of title, body of abstract and indexing annotation must be entered when the overall report is classified)

1. ORIGINATING ACTIVITY (Corporate author)	2a. REPORT SECURITY CLASSIFICATION
Information Systems a division of MBAssociates	Unclassified
	2b. GROUP

3. REPORT TITLE

Comparative Performance of Hollow-Cathode and Axial Plasma Helium Neon Lasers

4. DESCRIPTIVE NOTES (Type of report and inclusive dates)

Final Report

5. AUTHOR(S) (First name, middle initial, last name)

H. G. HEARD, Principal Investigator

A. J. PALMER, Project Engineer

6. REPORT DATE	7a. TOTAL NO. OF PAGES	7b. NO. OF REFS
March 1973	78	10

8a. CONTRACT OR GRANT NO	9a. ORIGINATOR'S REPORT NUMBER(S)
F33615-72-C-1323 b. PROJECT NO.	AFAL-TR-73-58
c.	9b. OTHER REPORT NO(S) (Any other numbers that may be assigned this report)
d.	IS-R-73/03

10. DISTRIBUTION STATEMENT

Distribution limited to U.S. Government agencies only; test and evaluation results reported: March 1973. Other requests for this document must be referred to ALAL/TEA, Wright-Patterson AFB, OH 45433.

11. SUPPLEMENTARY NOTES	12. SPONSORING MILITARY ACTIVITY
	Air Force Systems Command Air Force Avionics Laboratory Wright-Patterson AFB, Ohio 45418

13. ABSTRACT

This report covers a 12 month, primarily experimental investigation of the comparative performance characteristics of slotted hollow-cathode and axial plasma (positive column) 6328Å He-Ne lasers. The program included the evaluation of parameters that control power performance and culminated in the construction of a TEM_{00} mode power-optimized slotted hollow-cathode laser. The program was carried out in three main phases. First, a 15 mW TEM_{00} mode power-optimized axial plasma laser was constructed utilizing a 1-meter long folded confocal laser cavity. Second, a series of systematic parametric evaluations on the 6328Å laser oscillation of He-Ne-slotted hollow-cathode discharges using various cathode diameters was carried out using the same type of laser cavity. Among the most important observations made in this phase were: the inability, due to plasma expulsion from the cathode interior, to reach optimal operating pressure for maximum 6328Å output, consequently the power output and efficiency were lower than that of the 6328Å axial plasma laser; a sensitive dependence of performance on fractional slot width to cathode area; a quasi-periodic distribution of discharge erosion along the length of the cathode slot; and a comparatively high optimal He:Ne mixture ratio. Third, on the basis of the parametric evaluations, a TEM_{00} mode power-optimized slotted hollow-cathode laser was constructed using a 1-meter long folded-confocal laser cavity. The performance characteristics of this laser were: maximum TEM_{00} mode output power of 2 mW, optimal total operating pressure of 4 Torr, a He:Ne mixture ratio of 20:1 and nominal discharge current and tube voltage of 400 mA and 220 volts respectively.

DD FORM 1473

UNCLASSIFIED

Security Classification

KEY WORDS	LINK A		LINK B		LINK C	
	ROLE	WT	ROLE	WT	ROLE	WT
LASER,						
Hollow-Cathode						
Axial-Plasma						
All-Metal						
Low Voltage						
Low Power						
Rugged Construction						
Sputtering-Limited						
Computer-Design Codes						